PVlite

A simulator of PV systems applications

Modeling of solar radiation, PV components and systems in PVlite

Javier Muñoz Cano

Instituto de Energía Solar

Universidad Politécnica de Madrid

PVlite, version 2.3

https://blogs.upm.es/javiermunoz/

Author:

Javier Muñoz Cano.

Instituto de Energía Solar.

Universidad Politécnica de Madrid.

Department address:

Departamento de Ingeniería Eléctrica, Electrónica, Automática y Física Aplicada.

ETSI Diseño Industrial (ETSIDI).

C/ Ronda de Valencia, 3.

28012 Madrid (Spain).

Tel: +34 91 06 77567

Email: javier.munoz@upm.es

INDEX

1 Introduction

1-1 Overview

PVlite is a photovoltaic (PV) system simulator that has been developed for teaching purposes in several courses on PV systems engineering taught by the author.

This document describes the mathematical models and methods implemented in PVlite, which allows the simulation of common PV applications, such as grid-connected and stand-alone (off-grid) PV systems. The guide for executing and using PVlite is described in the user's manual.

1-2 History and programming languages

The first version of the simulator, called IESPRO (IES Productivity), was written in MatLab©. It was developed with the purpose of estimating the performance of grid-connected PV systems during the first Spanish boom (2006-2008), which was a demand of promoters and installers in those years.

IESPRO evolved during the following years to simulate the performance of emerging PV products that were being deployed in the market, such us different types of one-axis and two-axis solar trackers, which were being installed in large grid-connected PV plants. This demand required the development of new functionalities and models, such as the implementation of back-tracking strategies and the estimation of self-shading losses caused by adjacent static and sun-tracking PV generators.

In 2014, under the support of an European Project [1] the MatLab© version of IESPRO was translated to PHP for implementing a web version of the tool called SISIFO (Spanish acronym of Simulador de Sistemas Fotovoltaicos), which took the name of a previously symbol library of stand-alone PV components developed for OrCAD PSpice [2] A fossil of the first PHP source code of SISIFO, without graphical interfaces, can be still founded in the web [3] Later, in 2015, new models were developed for extending the capacity of IESPRO and SISIFO tools to the simulation of PV water pumping systems [4]

PVlite is a simplified and lightweight version of the previous simulators, which includes their basic models and applications (grid-connected and water pumping PV systems) but also it incorporates new functions, applications, and simulations options such as:

- Self-consumption in grid-connected systems.

- Stand-alone PV systems with ideal batteries.

- PV hybrid systems.

- Improved water pumping model.

The source code of PVlite, for MatLab© and Octave, this document and user's manual of this and subsequent versions can be downloaded from the institutional web page https://blogs.upm.es/javiermunoz/.

1-3 Contents of this document

This document is separated in several chapters with the following contents. Chapter 2 describes the fundamentals of solar radiation and temperature models, in particular the mathematical procedures for generating synthetic times series of solar irradiances and ambient temperatures starting from the 12 monthly-averages of the daily global horizontal irradiation and maximum and minimum ambient temperatures, which are the most common available information for any site.

Chapter 3 describes grid-connected PV systems and introduces power models for PV generators, inverters, and AC loads, which are common for all the PV applications simulated in PVlite.

Chapter 4 describes stand-alone PV systems with ideal batteries and chapter 5 water PV pumping systems. Finally, chapter 6 introduces the simulation of simple hybrid PV system with DC bus integrating a generator set and a wind turbine.

2 Solar radiation and temperature models

2-1 Introduction

PVlite performs yearly simulations of PV systems using as input data time series of solar horizontal irradiance and ambient temperature. For example, it allows using hourly TMY data coming from two popular databases, the Photovoltaic Geographical Information System (PVGIS) [4] and the National Solar Radiation Database (NSRDB) [6]

Besides, when these time series are not available, PVlite allows the generation of synthetic time series using methods described in this chapter, which require as input data monthly averages of daily irradiation on the horizontal plane and minimum and maximum ambient temperatures, which is an information usually available for any site.

The generation of time series of horizontal solar irradiance is performed using well-known methods described in the literature. On one side, a simpler approach called here "average days" generates a mean solar irradiance profile, which is the same for all the days of each month. On the other side, PVlite also allows to select a stochastic method, which generate a yearly synthetic series of daily clearness index and global horizontal solar irradiation.

After introducing these two synthetic methods, this chapter describes classic procedures for calculating, starting from horizontal irradiances, the incident solar radiation on both inclined static surfaces and typical one-axis and two-axis solar trackers.

2-2   Synthetic generation of solar radiation data

This section describes the methods for synthetizing time series of global, direct and diffuse irradiances on the horizontal plane starting from the twelve values of monthly-averaged global horizontal daily irradiation, called $G_{dm}(0)$.

In this point, it is worth introducing the nomenclature used in this document and the source code for naming and subscripting the components of solar radiation components and other simulated variables. The name of the variables is normally written in uppercase. For example, the components of solar

radiation on the inclined plane are called G (global), B (beam), D (diffuse) and R (reflected).

Each variable name may have two additional subscripts to indicate the period of integration and if it is an averaged value. The first subscript indicates the period of integration of the variable, which can be a day (d), a month (m) or an annual period (a). For lower periods of integration, such an hour, the subscript is omitted. The second subscript indicates that the value is an average over the period indicated by the subscript (d, m, or a).

Besides, the name of horizontal solar radiation components finishes with a zero written between parentheses (0), which indicates the horizontal collection plane. In the case of solar radiation components on an inclined surface the information on the inclination β and orientation α of the collection plane, which usually indicated as (β, α) after the variable, is not explicitly shown.

In the source code, which is written in plain text, the subscripts are lowercase letters that follows the variable name. And the horizontal surface is indicated with a zero (without parentheses). Table 1 shows examples of names of several variables.

Table 1.   Examples of names of several variables.

This document	Source code	Variable	Variable size
$G_{dm}(0)$	Gdm0	Monthly-averaged global horizontal daily irradiation, Wh/m²	1x12
B(0)	B0	Beam irradiance on the horizontal plane, W/m²	Nstepsx365 (*)
G	G	Global irradiance on the inclined plane, W/m²	Nstepsx365 (*)
G_d	Gd	Daily global irradiation on the inclined plane, Wh/m²	1x365
G_m	Gm	Monthly global irradiation on the inclined plane, Wh/m²	1x12
G_a	Ga	Annual irradiation on the inclined plane, Wh/m²	1x1

*Instantaneous values are considered constant during each simulation step, which can be selected from minutes to one hour maximum. Each instantaneous variable has *Nsteps* values per day, which depends on the simulation step. For example, *Nsteps*=24 for one hour simulation step.

Before going to description of the synthetic methods, next sections review some basic concepts on the motion earth-sun and present the equations implemented in the program for estimating several astronomical parameters, such as the distance earth-sun, the solar declination, and the position of the sun regarding horizontal or inclined planes, which are required for subsequent calculations.

2-2-1 Astronomical calculations

2-2-1-1 Motion sun-earth

The earth moves around the sun in an elliptical orbit where the sun is located at one of the foci. This orbit is contained in the so-called ecliptic plane, whose normal forms an angle of around 23.45º with the earth's polar axis (see Figure 1).
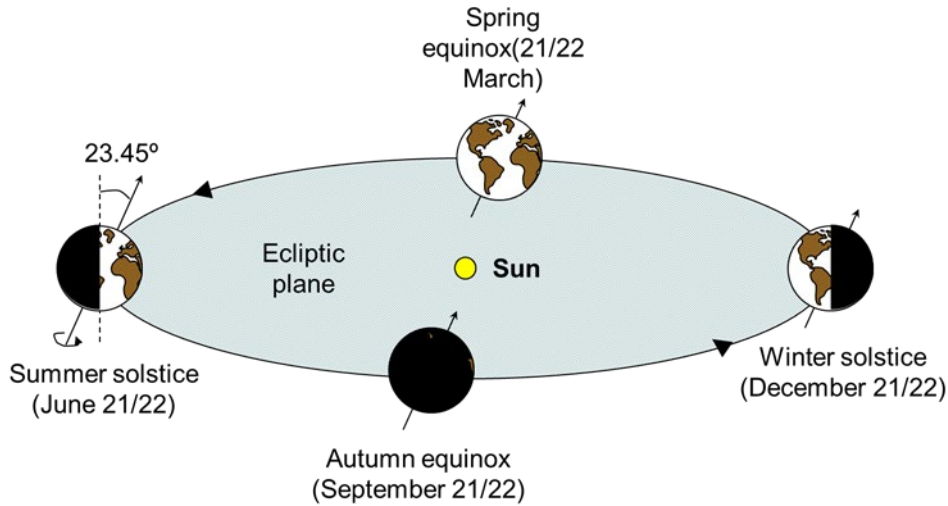

Figure 1. Elliptical orbit of the earth around the sun, which is contained in the so-called ecliptic plane.

The magnitude of solar radiation the reaches the earth is inversely proportional to the square of the distance sun-earth r and therefore their variation should be estimated throughout the year. For subsequent calculations, it is convenient to express this distance by means of a related parameter called eccentricity correction factor of the earth's orbit ε_0, which is calculated using the equation proposed by Spencer [7]

$$\varepsilon_0 = \left(\frac{r_0}{r}\right)^2 = 1.00011 + 0.034221 \cdot \cos(\Gamma) + 0.001280 \cdot \sin(\Gamma) \qquad (1)$$
$$+ 0.000719 \cdot \cos(2\Gamma) + 0.000077 \cdot \sin(2\Gamma)$$

Where r_0 is called one astronomical unit ($r_0 = 1\ AU = 1{,}496 \cdot 10^8\ km$) and Γ is called the day angle, as defined in Iqbal [8] which is calculated in radians as

$$\Gamma = (d_n - 1)\frac{2\pi}{365} \qquad (2)$$

Where d_n is the day of the year, which varies from 1 to 365. The Figure 2 shows the variation of the eccentricity correction factor as function of d_n. The minimum sun-earth distance is called perihelion ($r \cong 0.983\ AU$) and occurs on 3

January ($d_n = 3$). The maximum distance is the aphelion ($r \cong 1.017\ AU$) and occurs on 5 July ($d_n = 186$).
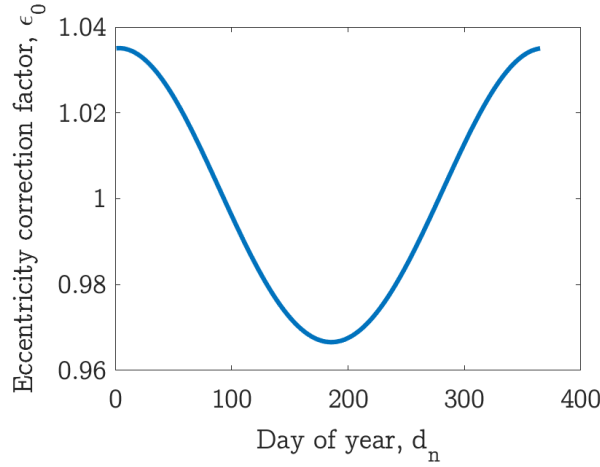

Figure 2. Variation of the eccentricity correction factor as function of the day of year.

Other required parameter for calculations is the solar declination δ, which is the angle formed by the equatorial plane with the straight line joining the centers of the earth and the sun. This angle changes instantly, but it can be assumed it is approximately constant during every day with negligible error. The solar declination, in radians, is estimated using other expression proposed by Spencer [8]

$$\delta = 0.006918\text{-}0.399912\cos(\Gamma) + \qquad (3)$$
$$0.070257\text{sen}(\Gamma)\text{-}0.006758\cos(2\Gamma) +$$
$$0.000907\text{sen}(2\Gamma)\text{-}0.002697\cos(3\Gamma) + 0.00148\text{sen}(3\Gamma)$$

Where δ is given in radian and Γ is the day angle as defined above. The Figure 3 shows the variation of the solar declination as function of the day of the year, and the Figure 4 its relevant values during the equinoxes and the solstices.
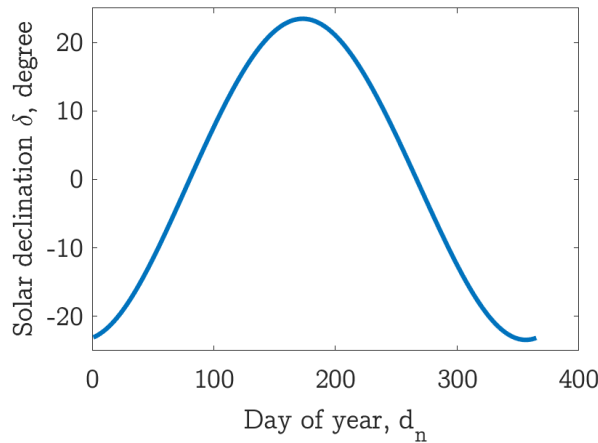

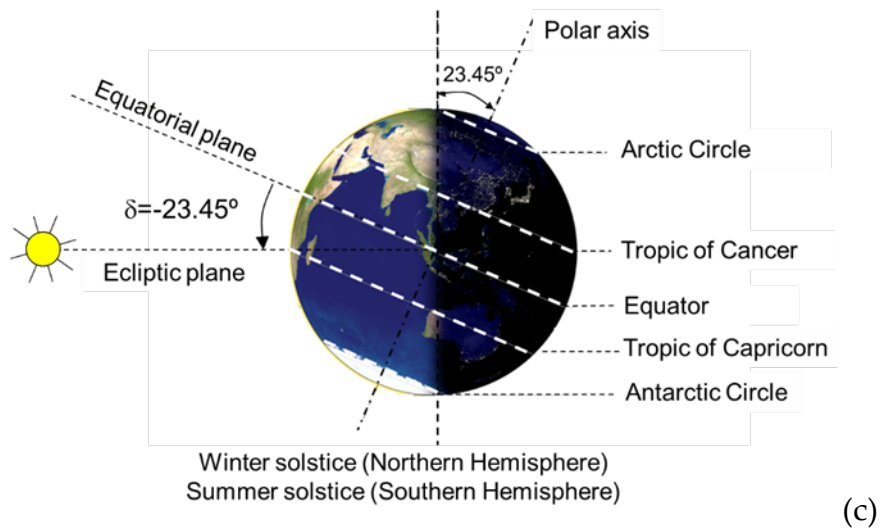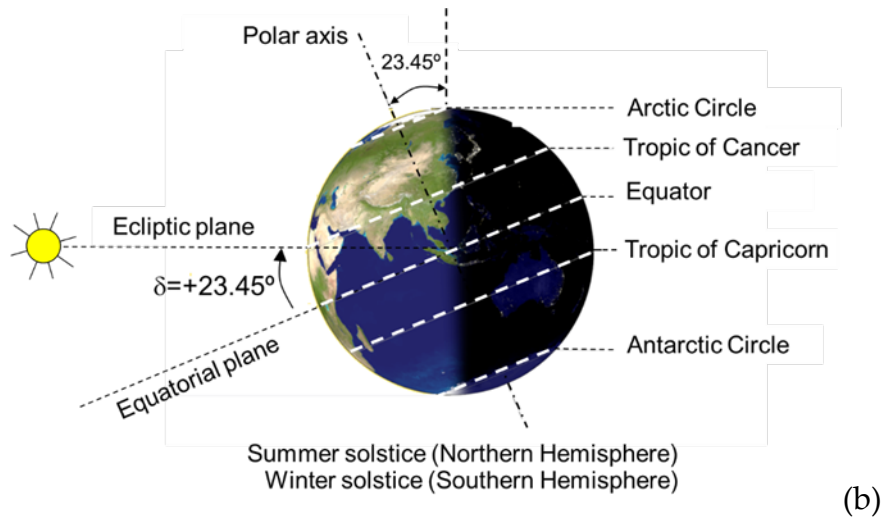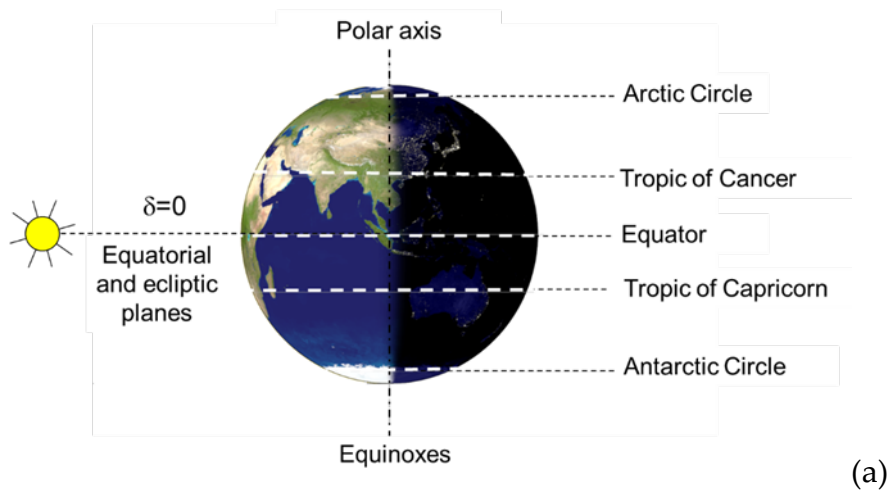*Figure 3. Variation of the solar declination, in degree, as function of the day of year.*

10

Figure 4. Relevant values of the solar declination throughout the year.
(a) Equinoxes, $\delta = 0$. (b) Summer solstice (Northern Hemisphere, NH), $\delta = 23.45^{\circ}$. (c) Summer solstice (Southern Hemisphere, SH), $\delta = -23.45^{\circ}$.

The synthetic methods described below generate time series of solar radiation using as reference the true solar time ω, which is an angle that indicates the difference between the local midday ($\omega = 0$), when the sun is over the local meridian, and other instant of the day in terms of earth rotation of 15º per hour (360º per day). Defining the local midday at 12 hours, the conversion between a given solar hour h and ω in radians is given by

$$\omega = 15(h - 12)\frac{\pi}{180} \tag{4}$$

PVlite also accepts as input data hourly time series of TMY data coming from several databases that use as reference the local standard time, i.e., the time on the clock. For using such data, it is necessary convert from local standard time to true solar time, which requires, amongst other calculations, to estimate the value of the equation of time ET, which is the deviation between the clock time, when the local midday is expected, and the real instant when the sun is over the local meridian.

The equation of time is calculated throughout the year, in radians, using other expression proposed from Spencer [7]

$$\begin{aligned}
ET = 0.000075 &+ 0.001868\,cos\,\Gamma \\
&- 0.032077\,sin\,\Gamma \\
&- 0.014615\,cos\,(2\Gamma) \\
&- 0.040849\,sin\,(2\Gamma)
\end{aligned} \tag{5}$$

The Figure 5 shows the variation of the equation of time as function of the day of the year. The minimum value is around -14 minutes on February 14 ($d_n = 45$) and the maximum +16 minutes on November 2 ($d_n = 306$).
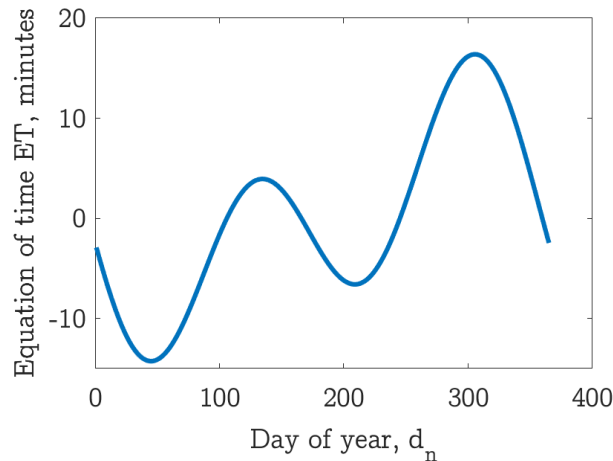

Figure 5. *Variation of the solar declination as function of the day of year.*

Finally, it is worth mentioning that the previous equations have other simpler mathematical forms, though less accurate, which are more practical for hand-made calculations [8] [9]

2-2-1-2 Position of the sun relative to the horizontal surface

For an observer on the earth surface, the position of the sun in the celestial sphere can be described by two of the angles displayed in Figure 6. The solar zenith angle θ_{ZS}, also called the solar zenith distance, is the angle between the zenith (normal to the earth's surface at the observer location) and the line that joints the observer and the sun. The solar zenith angle varies between 0º and 90º. The complement of the solar zenith angle is called the solar altitude γ_S.

The third angle is the solar azimuth ψ_S, which is the angle between the local meridian, facing towards the equator, and the projection on the earth's surface of the line that joints the observer and the sun. This angle is zero at noon and it is defined as negative towards the East (in the morning) and positive towards the West (in the afternoon).
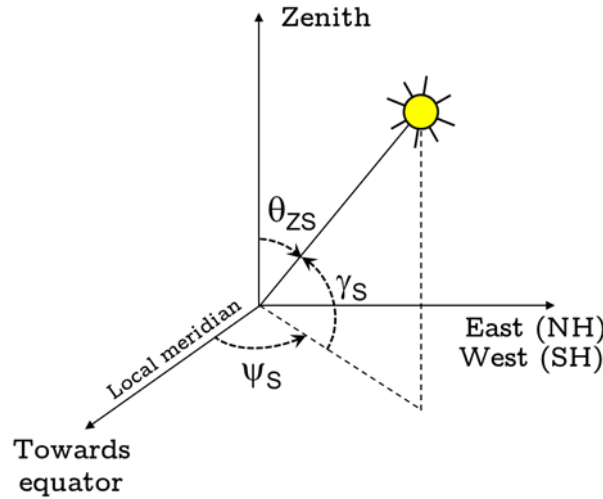
Figure 6. Definition of the position of the sun on the celestial sphere relative to an observer located at the origin of coordinates facing towards the equator.

For a given location at the earth's surface, the solar zenith and solar azimuth angles are given by the following relations [9]

$$\cos\theta_{ZS} = \sin\delta\sin\phi + \cos\delta\cos\phi\cos\omega = \sin\gamma_S \tag{6}$$

$$\cos\psi_S = \frac{(\sin\gamma_S\sin\phi - \sin\delta)}{\cos\gamma_S\cos\phi}[\text{sign}(\phi)] \tag{7}$$

Where ϕ is the latitude of the location, defined as north positive and south negative, and ω is the true solar time, which is zero at noon and it is defined as negative towards the east and positive towards the west.

From the previous equations, the sunrise hour angle ω_S is obtained for $\gamma_S = 0º$ as

$$\omega_S = -arccos(-tan\delta tan\phi) \tag{8}$$

This solar angle is negative as defined above. From this value, the sunset hour angle is obtained as $|\omega_S|$ and the duration of the day as $|2\omega_S|$. It is worth noting that, for polar regions, the previous equation yields a $cos\omega_S > 1$ during the winter (the sun does not rise) and $cos\omega_S < -1$ during the summer (the day is continuous). In these cases, for simulation purposes is convenient to set, respectively, $\omega_S = 0$ and $\omega_S = -\pi$.

2-2-2 Average days

2-2-2-1 Extraterrestrial radiation

The solar constant $B_0 = 1367 \text{ W/m}^2$ is the irradiance (incident power per unit area) perpendicular to the sun's rays when the sun-earth distance is 1 AU. The variation of this distance throughout the year leads to small changes of the normal incident irradiance $B_0(n)$, which can be calculated using the following expression

$$B_O(n) = B_O \left(\frac{r_0}{r}\right)^2 = B_O \cdot \varepsilon_0 \tag{9}$$

Where ε_0 is the eccentricity correction factor of the earth's orbit, estimated using equation (1). In the perihelion $(r_0/r)^2 \cong 1.035$ and in the aphelion $(r_0/r)^2 \cong 0.967$, hence the normal irradiance can vary as much 3.5%.

The extraterrestrial irradiance collected by a horizontal surface (see Figure 7) is obtained as

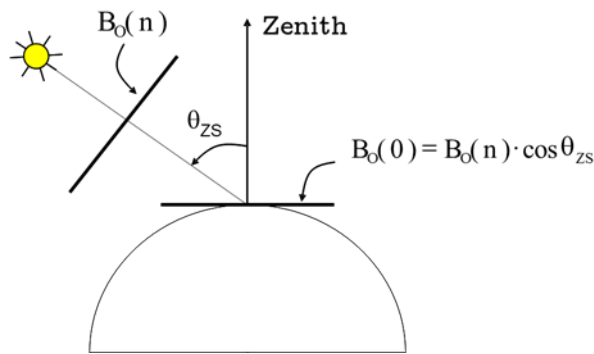$$B_O(0) = B_O \cdot \varepsilon_0 \cdot cos\,\theta_{ZS} \tag{10}$$

Figure 7. Irradiance collected by a horizontal surface outside the atmosphere.

The extraterrestrial daily horizontal irradiation $B_{0d}(0)$ can calculate as

$$B_{Od}(0) = \int_{Sunrise}^{Sunset} B_O \cdot \varepsilon_0 \cdot cos\,\theta_{ZS}\,dt = \tag{11}$$

$$= 2 \cdot \int_{Sunrise}^{Noon} B_O \cdot \varepsilon_0 \cdot cos\,\theta_{ZS}\,dt$$

Assuming that ε_0 is constant during every day and performing a change of variable from t to ω (at 15 degree per hour, in radians, $dt = (12/\pi)d\omega$) the previous equation can be expressed as

$$B_{Od}(0) = \frac{24}{\pi} \cdot B_O \cdot \varepsilon_0 \int_{-\omega_S}^{0} \cos\theta_{ZS}\, d\omega \tag{12}$$

$$B_{Od}(0) = \frac{24}{\pi} \cdot B_O \cdot \varepsilon_0 \int_{-\omega_S}^{0} (\sin\delta\sin\phi + \cos\delta\cos\phi\cos\omega)d\omega \tag{13}$$

Whose result is

$$B_{Od}(0) = \frac{24}{\pi} \cdot B_O \cdot \varepsilon_0[-\omega_S \sin\delta\sin\phi - \cos\delta\cos\phi\sin\omega_S] \tag{14}$$

Where ω_S is negative and expressed in radians. The Figure 8 shows the calculation of the extraterrestrial daily horizontal irradiation collected by a horizontal surface in Madrid ($\phi = 40.7°$) using the previous equation.
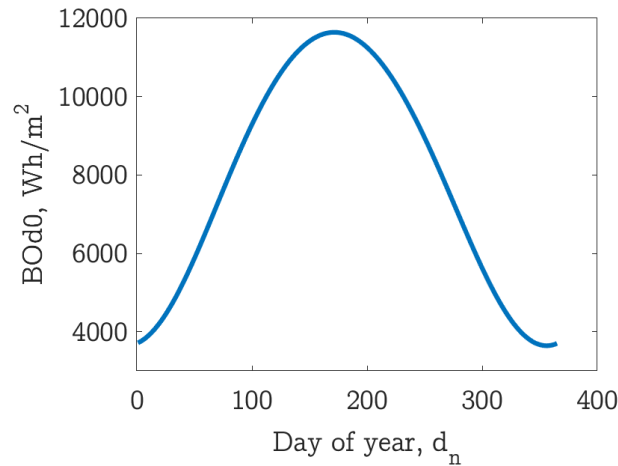
Figure 8. *Extraterrestrial daily horizontal irradiation collected by a horizontal surface in Madrid ($\phi = 40.7°$).*

The monthly average of the extraterrestrial daily irradiation $B_{Odm}(0)$ is calculated for a given month as

$$B_{Odm}(0) = \frac{1}{Month\ length} \sum_{Month} B_{Od}(0) \tag{15}$$

It worth mentioning that for each month there is a day, called characteristic day, whose solar declination is approximates the average solar declination of that month δ_{dm} and verifies that $B_{Od}(0) \cong B_{Odm}(0)$. Table 2 shows the solar declination of the characteristic days of each month obtained for Madrid ($\phi = 40.7°$) using the equations described in this chapter[8] Characteristic days vary slightly with the latitude. For example, the characteristic days indicated in

Iqbal [6] are calculated for $\phi = 35^{\circ}$ and vary one day for some months (see last column of Table 2).

Month	Month length	Characteristic days		Declination, degree		Extraterrestrial irradiation, Wh/m²		d_n [6]
		Date	d_n	δ (d_n)	δ_{dm}	$B_{0d}(0)$ (d_n)	$B_{0dm}(0)$	
January	31	17	17	-20.90	-20.82	4118	4133	17
February	28	15	46	-12.95	-13.01	5609	5598	45
March	31	16	75	-2.04	-2.03	7616	7611	74
April	30	15	105	9.48	9.56	9586	9591	105
May	31	15	135	18.67	18.70	10997	10995	135
June	30	11	162	23.04	23.05	11596	11592	161
July	31	17	198	21.35	21.26	11306	11295	199
August	31	17	229	13.67	13.84	10131	10153	230
September	30	17	260	2.57	3.11	8309	8395	261
October	31	18	291	-9.33	-8.51	6204	6349	292
November	30	17	321	-18.81	-18.23	4472	4580	322
December	31	12	346	-23.02	-22.96	3713	3724	347

Table 2.   Solar declination of the characteristic days of each month calculated for Madrid ($\phi = 40.7^{\circ}$) using the previous equations. The last column displays the characteristic days indicated in Iqbal for $\phi = 35^{\circ}$ [6].

2-2-2-2 Clearness index

The clearness index K_T is defined as the ratio of global solar radiation on the earth's surface and the extraterrestrial horizontal radiation. For example, the monthly average of the daily clearness index, which is equal to the monthly clearness index, is expressed as

$$K_{Tdm} = K_{Tm} = \frac{G_{dm}(0)}{B_{0dm}(0)} \tag{16}$$

The clearness index allows to characterize the statistical properties of the solar radiation [10] it is the basis for calculating the solar radiation on inclined surfaces.

2-2-2-3 Generation of horizontal irradiances

The first step of the synthetic method consists of assigning to all days of a given month the monthly average of daily global horizontal irradiation $G_d(0) = G_{dm}(0)$. The result is very similar if the simulations are performed only for the characteristic day of each month, which reduces computing time. Nevertheless, the first approach is used here to ensure its compatibility with other PVlite algorithms, such as the Aguiar method described below or the use of TMY time series, which requires to simulate with all the days of the year.

The next step is the calculation of the daily clearness index

$$K_{Td} = \frac{G_d(0)}{B_{Od}(0)}$$ (17)

Which allows to obtain the daily diffuse fraction K_{Dd} of the horizontal irradiation. For that, it is assumed here that daily diffuse fraction of individual days of a given month is the same and equal to the monthly diffuse fraction ($K_{Td} = K_{Tm}$). The latter is estimated using different monthly empirical correlations, which can be selected by the user amongst the expressions proposed by

1. Page [11]

$$K_{Dd} = 1 - 1.13K_{Td}$$ (18)

2. Collares-Pereira and Rabl [12]

$$K_{Dd} = 0.775 + 0.347\left(|\omega_S| - \frac{\pi}{2}\right)$$ (19
$$- \left[0.505 + 0.261\left(|\omega_S| - \frac{\pi}{2}\right)\right]cos(2(K_{Td} - 0.9))$$

3. Erbs [13]

$$K_{Dd} = 1.391\text{-}3.56{\cdot}K_{Td}{+}4.189{\cdot}K_{Td}^2\text{-}2.137{\cdot}K_{Td}^3 \quad |\omega_S| \leq 1.4208 \ rad$$ (20)

$$K_{Dd} = 1.311\text{-}3.022{\cdot}K_{Td}{+}3.427{\cdot}K_{Td}^2\text{-}1.821{\cdot}K_{Td}^3 \ |\omega_S| > 1.4208 \ rad$$

4. Macagnan, for Madrid [14]

$$K_{Dd} = 0.758\text{-}0.428{\cdot}K_{Td}\text{-}0.503{\cdot}K_{Td}^2$$ (21)

Once the daily fraction is obtained, the daily horizontal irradiation components, diffuse $D_d(0)$ and beam $B_d(0)$ of the global daily irradiation $G_d(0)$ are calculated as

$$D_d(0) = K_{Dd} \cdot G_d(0)$$ (22)

$$B_d(0) = (1 - K_{Dd}) \cdot G_d(0)$$ (23)

Finally, for estimating the instantaneous irradiance from these daily irradiation components it is worth calculating first the ratio between the horizontal extraterrestrial irradiance $B_O(0)$ and the horizontal extraterrestrial daily irradiation $B_{Od}(0)$, which can be obtained from equations (6), (10) and (14) as:

$$\frac{B_O(0)}{B_{Od}(0)} = \frac{\pi}{24} \cdot \frac{cos\ \omega - cos\ \omega_S}{\omega_S\ cos\ \omega_S - sin\omega_S}$$ (24)

Where ω_S is negative and expressed in radians. From experimental observations, Liu and Jordan [10] found that the ratio between $D(0)$ and $D_d(0)$ matches very well to the last equation

$$r_d = \frac{D(0)}{D_d(0)} = \frac{\pi}{24} \cdot \frac{\cos\omega - \cos\omega_S}{\omega_S \cos\omega_S - \sin\omega_S} \tag{25}$$

Lately, Collares-Pereira and Rabl [12] proposed a similar expression for the ratio between $G(0)$ and $G_d(0)$ with a small correction that depends on the instant of the day:

$$r_g = \frac{G(0)}{G_d(0)} = \frac{\pi}{24} \cdot \frac{\cos\omega - \cos\omega_S}{\omega_S \cos\omega_S - \sin\omega_S}(a + b\cos\omega) \tag{26}$$

Where the parameters a and b are calculated using the following equations:

$$a = 0.409\text{-}0.5016\sin(\omega_S + 1.047) \tag{27}$$
$$b = 0.6609 + 0.4767\sin(\omega_S + 1.047)$$

Once the normalized profiles of r_d and r_g are calculated, the three instantaneous irradiance components of the solar horizontal radiation are obtained as:

$$G(0) = r_g G_d(0) \tag{28}$$

$$D(0) = r_d D_d(0)$$

$$B(0) = G(0) - D(0)$$

2-2-3 Procedure for generating synthetic daily sequences of global horizontal irradiation

PVlite also allows the generation of daily sequences of global irradiation using as input data the monthly average of daily horizontal global irradiation $G_{dm}(0)$ and implementing the procedure proposed by Aguiar et al. which is based on a library of Markov transition matrices.

The procedure generates for a synthetic yearly sequence of 365 daily clearness index K_{Td} starting from the twelve values of K_{Tdm}. The monthly average of the synthetic K_{Td} series deviates from K_{Tdm} within a predefined range, which is established by default in $K_{Tdm} \pm 1\%$.

Once the K_{Td} synthetic series has been generated, the global daily irradiation is calculated as

$$G_d(0) = K_{Td}B_{Od}(0) \tag{29}$$

Finally, the diffuse horizontal irradiation components $D_d(0)$ and $B_d(0)$, as well the instantaneous horizontal irradiances $G(0)$, $D(0)$ and $B(0)$ are calculated using the procedure described in the previous section.

Figure 9 shows of an example of a synthetic series of daily global horizontal irradiation generated for Madrid using the Aguiar procedure and the clearness index K_{Tdm} indicated in Table 3.
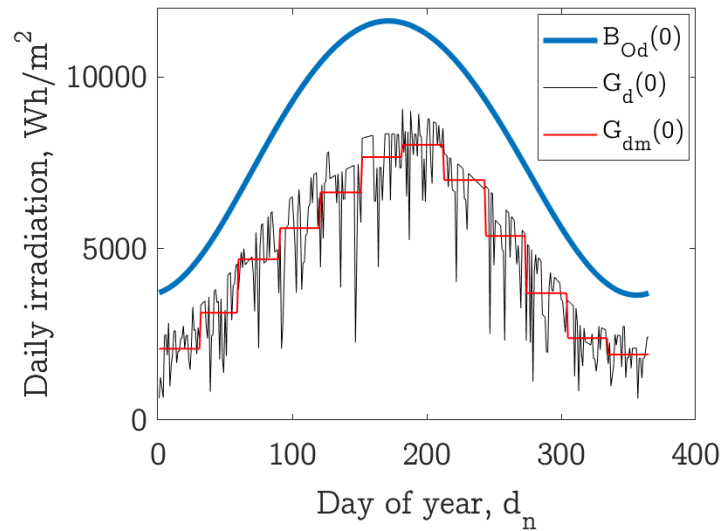

Figure 9. Example of a synthetic series of daily global horizontal irradiation generated for Madrid using the Aguiar procedure and the clearness index K_{Tdm} indicated in Table 3.

Month	$G_{dm}(0)$ Wh/m²	$B_{Odm}(0)$ Wh/m²	K_{Tdm}	T_{mm} ºC	T_{Mm} ºC
January	2080	4133	0.503	3	10
February	3130	5598	0.559	3.1	12.7
March	4690	7611	0.616	5.3	16.3
April	5600	9591	0.584	6.2	17.8
May	6640	10995	0.604	10.2	22
June	7670	11592	0.662	15.1	29
July	8030	11295	0.711	17	31.7
August	7000	10153	0.689	16.5	31.2
September	5370	8395	0.640	13.3	26.1
October	3700	6349	0.583	10.4	20.2
November	2390	4580	0.522	6.1	13.3
December	1910	3724	0.513	3.4	10

Table 3.   Monthly average of several daily parameters for Madrid.

2-3 Procedure for generating daily profiles of ambient temperature

The procedure implemented in PVlite generates daily sequences of ambient temperature, which are the same for all the days of each month, starting from the monthly averages of daily minimum T_{mm} and maximum T_{Mm} ambient temperatures.

The model assumes that the minimum temperature occurs at sunrise ($\omega = \omega_S$) and the maximum two hours after midday ($\omega = \pi/6$), and interpolates between these two points by cosines functions [9] The equations of the model for a given day are the following.

- Interval $(-\pi < \omega \le \omega_S)$

$$T_a = T_{Mm} - \left(\frac{T_{Mm} - T_{mm}}{2}\right)(1 + \cos(a_T\omega + b_T))$$

Where

$$a_T = -\pi/(\omega_S + 11\pi/6)$$
$$b_T = -a_T\omega_S$$

- Interval $(\omega_S < \omega \le \pi/6)$

$$T_a = T_{mm} + \left(\frac{T_{Mm} - T_{mm}}{2}\right)(1 + \cos(a_T\omega + b_T))$$

Where

$$a_T = \pi/(\omega_S - \pi/6)$$
$$b_T = -a_T\omega_S$$

- Interval $(\pi/6 < \omega \le \pi)$

$$T_a = T_{Mm} - \left(\frac{T_{Mm} - T_{mm}}{2}\right)(1 + \cos(a_T\omega + b_T))$$

Where

$$a_T = \pi/(\omega_S + 11\pi/6)$$
$$b_T = -(\pi + a_T\pi/6)$$

Figure 10 displays an example of the generated daily sequences of ambient temperature obtained for Madrid using the monthly average minimum T_{mm} and maximum T_{Mm} ambient temperatures indicated in Table 3. Each bundle of curves corresponds to one month.
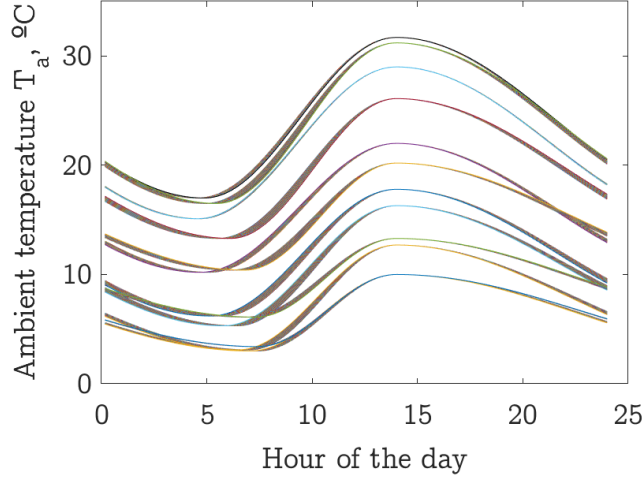
Figure 10. Daily sequences of ambient temperature generated for Madrid using the monthly average minimum T_{mm} and maximum T_{Mm} ambient temperatures indicated in Table 3. Each bundle of curves corresponds to one month.

2-4 Simulations with TMY data

PVlite also allows the use of hourly series TMY data files downloaded from the popular databases PVGIS [4] and NSRDB [6] Both databases directly provide hourly values of global and diffuse irradiances on the horizontal surface, and beam irradiances are calculated as the difference between both components.

These databases also provide other hourly data required for simulation, such as ambient temperatures and the wind speed, which is used for simulating hybrid PV-wind systems.

PVlite also calculates the monthly average of daily irradiation components and minimum and maximum ambient temperatures extracted from the TMY, which allows performing simulations using the procedures described in previous sections.

2-5 Calculation of the radiation on inclined surfaces

Once the instantaneous irradiances on the horizontal surface: global ($G(0)$, beam $B(0)$, and diffuse $D(0)$ components are either generated or obtained from databases, PVlite calculates the global incident irradiance G on inclined surfaces (static, one axis, and two axis trackers) as

$$G = B + D + R \tag{31}$$

Where B, D, and R are the beam, diffuse and reflected irradiance components on the inclined surface, which are calculated using classic procedures described in this section. As mentioned above, for simplicity, the nomenclature of these variables omits information on the position of the inclined surface, which can be described by its inclination β, or slope, regarding the

horizontal, and by its azimuth α, which is defined as the angle between the local meridian and the projection on the horizontal of the normal to the surface $\hat{n}$, as displayed in Figure 11. By convention, similarly to the solar azimuth, the value of α is zero at noon, negative towards the East (in the morning) and positive towards the West (in the afternoon).

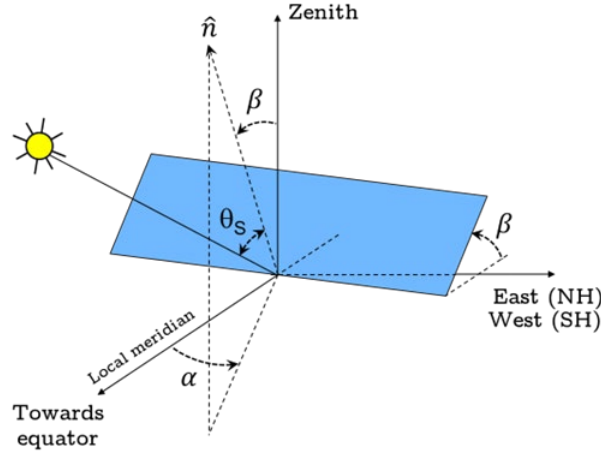*Figure 11. Position of the inclined surface relative to the horizontal.*

For subsequent calculations is necessary to estimate the incidence angle θ_S between the normal to the surface $\hat{n}$ and the line that joints the origin and sun position (see Figure 11).

2-5-1 Calculation of the angle of incidence

Using a cartesian coordinate system OXYZ with the origin placed in the location with the axis X, Y, Z pointing to West (East in SH), South (North in SH) and Zenith, respectively, the coordinates of the unit vector of the sun can be expressed as

$$
\begin{aligned}
x_{sun} &= \cos \gamma_S \cdot \sin \psi_S \\
y_{sun} &= \cos \gamma_S \cdot \cos \psi_S \\
z_{sun} &= \sin \gamma_S
\end{aligned}
\tag{32}
$$

In the same coordinate system, the unit vector of the normal to surface is given by

$$
\begin{aligned}
x_{surf} &= \sin \beta \cdot \sin \alpha \\
y_{surf} &= \sin \beta \cdot \cos \alpha \\
z_{surf} &= \cos \beta
\end{aligned}
\tag{33}
$$

Finally, the cosine of the angle of incidence is obtained as the scalar product of theses unit vectors.

$$
\cos \theta_S = x_{sun} x_{surf} + y_{sun} y_{surf} + z_{sun} z_{surf}
\tag{34}
$$

2-5-2 Angles for solar trackers

Besides static surfaces, PVlite also calculates the incident solar radiation on three solar trackers:

- One axis North-South horizontal. The rotating axis is parallel to the local meridian (see Figure 12-a).
- One axis azimuthal. The rotating axis is vertical (see Figure 12-b).
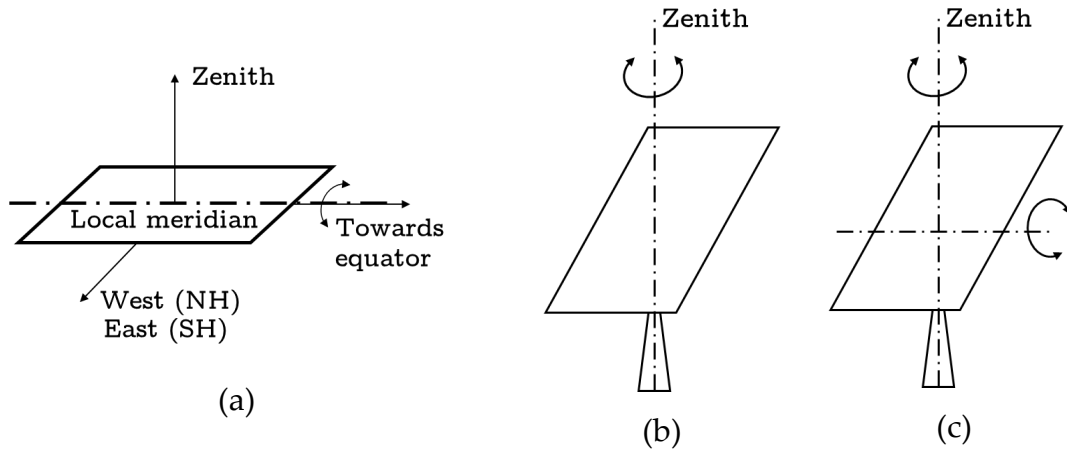- Two axes. The surface is always perpendicular to the sun rays (see Figure 12-c).

Figure 12. Solar trackers simulated in PVlite. (a) One axis North-South horizontal (b) One axis vertical (azimuthal). (c) Two axes.

For one axis North-South horizontal, the azimuth of the surface is given by

$$\alpha = \begin{cases} -90^{\varrho} & \psi_S \le 0 \\ +90^{\varrho} & \psi_S > 0 \end{cases} \tag{35}$$

The cosine of the angle of incidence is calculated as

$$cos\,\theta_S = cos\,\gamma_S \cdot |sen\psi_S| \cdot sen\beta + sen\gamma_S \cdot cos\,\beta \tag{36}$$

And the inclination that β minimizes θ_S is obtained from

$$tan\,\beta = \frac{|sen\psi_S|}{tan\,\gamma_S} \tag{37}$$

For one axis azimuthal solar tracker the inclination β is constant, which should be optimized for each location, the azimuth is $\alpha = \psi_S$, and the angle of incidence is given by

$$\theta_S = |\theta_{ZS} - \beta| \tag{38}$$

Finally, for a two-axes tracker $\alpha = \psi_S$, $\beta = \theta_{ZS}$, and $\theta_S = 0$.

2-5-3 Calculation of the beam irradiance

The beam, or direct component, of the inclined surface is calculated (see Figure 13) as

$$B = \frac{B(0)}{\cos\theta_{ZS}} max[0, \cos\theta_S]$$ (39)

When the sun is behind the collection surface, the angle of incidence is higher than 90º. Hence, since $\cos\theta_S < 0$, the maximum between zero and $\cos\theta_S$ is zero and, therefore, $B = 0$.
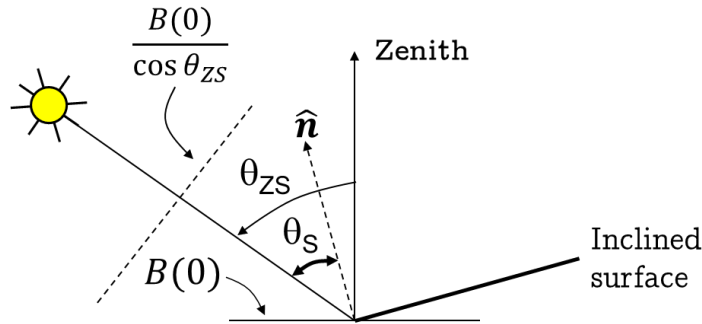

Figure 13. Calculation of the beam irradiance.

2-5-4 Calculation of the diffuse irradiance

The diffuse irradiance is calculated using three models that can be selected by the user: the simple isotropic model and the anisotropic models proposed by Hay and Davies [16] and Perez [17]

The isotropic model calculates the diffuse irradiation, assuming the radiation is uniform from any point of the celestial sphere, using the expression:

$$D = D(0)\frac{1 + \cos\beta}{2}$$ (40)

This model is included just for completeness, since its use is not recommended because it underestimates the diffuse irradiance on surfaces oriented towards the equator [9] In general, anisotropic models provide better results.

The model of Hay and Davies considers that diffuse irradiance is composed by two components, one isotropic D_{ISO} and other circumsolar D_{CIR}, which can be treated as the beam irradiance

$$D = (1 - k_1)D(0)\frac{1 + \cos\beta}{2} + k_1\frac{D(0)}{\cos\theta_{ZS}} max[0, \cos\theta_S]$$ (41)
$$= D_{ISO} + D_{CIR}$$

The weight of each component depends on the anisotropy index k_1, which is defined as

$$k_1 = \frac{B(0)}{B_O(0)} = \frac{B(0)}{B_0 \varepsilon_0 \cos \theta_{ZS}}$$

(42)

Note that the isotropic model is obtained for $k_1 = 0$, which would occur under overcast sky conditions.

The Perez model considers three diffuse irradiance components: isotropic, circumsolar and an additional component coming from the horizon band

$$D = D(0) \left[(1 - k_1) \frac{1 + \cos \beta}{2} + \frac{k_1}{\cos \theta_{ZS}} max[0, \cos \theta_S] \right. \\ \left. + k_2 sen\beta \right]$$

(43)

Where k_1 and k_2 are experimental parameters. It is worth mentioning that the Perez model requires the calculation of air mass (AM), which is estimated by PVlite using the ESRA model [18]

2-5-5 Calculation of the reflected irradiance

The last component of the global irradiance comes from the reflection of the solar radiation on the ground, which can be estimated, assuming the ground is horizontal and reflects isotropically as

$$R = \rho G(0) \frac{1 - \cos \beta}{2}$$

(44)

Where ρ is the reflectivity of the ground, which can be selected by the user and whose value by default is $\rho = 0.2$.

2-5-6 Calculation of the global effective irradiance

Finally, PVlite calculates the global effective irradiance G_{ef} on the inclined surface, which is equal to the incident irradiance G less optical losses caused by the angle of incidence and dust, which are estimated using the Martin and Ruiz model [19] [20]

The expression of the angular losses $AL(\theta_S)$, defined with reference to normal incidence ($AL(0) = 0$) is given by

$$AL(\theta_S) = 1 - \frac{1 - exp\left[-(cos\theta_S)/a_r \right]}{1 - exp\left(-1/a_r \right)}$$

(45)

Where a_r is the angular loss coefficient, an experimental parameter that depends on each PV module technology. These angular losses increase by

accumulation of dust thickness on the surface of the PV modules. The accumulation of dust can be characterized by a transmittance factor FT at normal incidence and by a higher value of a_r, whose typical value is 0.17 for a clean surface and can increase up to 0.27 for a high amount of accumulated dust [19].

The effective irradiance is calculated as

$$G_{ef} = B_{ef} + D_{ef} + R_{ef} \tag{46}$$

Where B_{ef}, D_{ef}, and R_{ef} are the effective values of the beam, diffuse and reflected incident irradiances, which are calculated using the following expressions:

$$B_{ef} = B \cdot (1 - F_B(\theta_S)) \cdot FT \tag{47}$$

$$D_{ef} = [D_{CIR}(1 - F_B(\theta_S)) + D_{ISO}(1 - F_D(\beta))] \cdot FT \tag{48}$$

$$R_{ef} = R \cdot (1 - F_R(\beta)) \cdot FT \tag{49}$$

Where:

$$F_B(\theta_S) = \frac{exp[-(cos\theta_S)/a_r] - exp\,(-1/a_r)}{1 - exp\,(-1/a_r)} \tag{50}$$

$$F_D(\beta) \cong exp\left(-\frac{1}{a_r}\left[c_1\left(\sin\beta + \frac{\pi - \beta - \sin\beta}{1 + \cos\beta}\right)\right.\right. \tag{51}$$
$$\left.\left. + c_2\left(\sin\beta + \frac{\pi - \beta - \sin\beta}{1 + \cos\beta}\right)^2\right]\right)$$

$$F_R(\beta) \cong exp\left(-\frac{1}{a_r}\left[c_1\left(\sin\beta + \frac{\beta - \sin\beta}{1 - \cos\beta}\right)\right.\right. \tag{52}$$
$$\left.\left. + c_2\left(\sin\beta + \frac{\beta - \sin\beta}{1 - \cos\beta}\right)^2\right]\right)$$

The value of the coefficient c_1 is $4/(3\pi)$ and the coefficient c_2 is a fitting parameter. For simulations, four levels of dust can be selected, which are characterized by the parameters indicated in Table 4.

Level of dust	FT	a_r	c_1	c_2
Clean (0%)	1	0.17	$4/(3\pi)$	-0.069
Low (2%)	0.98	0.20	$4/(3\pi)$	-0.054
Medium (3%)	0.97	0.21	$4/(3\pi)$	-0.049
High (8%)	0.92	0.27	$4/(3\pi)$	-0.023

Table 4.   Set of parameters for the model depending on the degree of dust selected for simulation.

3 Grid-connected PV systems

3-1 Introduction

The configuration of the grid-connected PV system simulated in PVlite is displayed in Figure 14, whose main components are a PV generator, a maximum power point tracker (MPPT), and an inverter. The MPPT and the inverter are displayed as separate elements but in practice they are included in the same power converter.

The output power of the inverter supplies local AC loads and the surplus is exported to the power grid. Before of describing the operation of this system (section 3-5), next sections introduce the power models of the PV generator, the inverter and AC loads implemented in PVlite, which are the same for simulating other PV system applications.
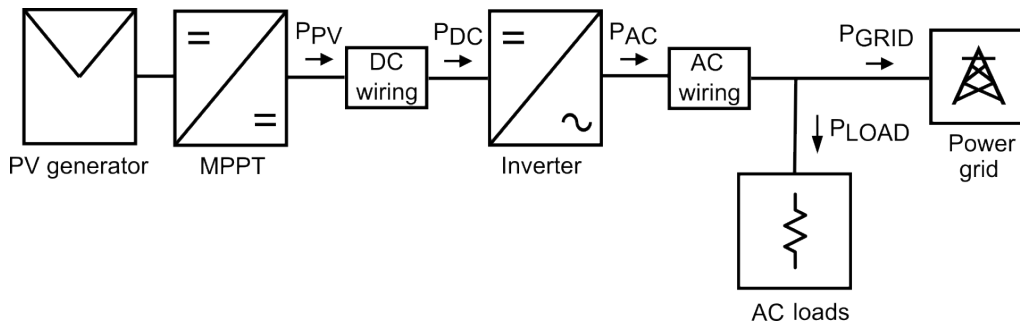

Figure 14. Grid-connected PV system simulated in PVlite.

3-2 PV generator model

The maximum power of a PV generator under Standard Test Conditions (STC) P_{PV}^* is given by

$$P_{PV}^* = \eta_{PV}^* \cdot A \cdot G^* \tag{53}$$

Where η_{PV}^* is PV generator efficiency under STC, A is the PV generator area and $G^* = 1,000\ Wm^{-2}$. For operating conditions different from STC, the maximum power of the PV generator P_{PV} can be calculated similarly as

$$P_{PV} = \eta_{PV} \cdot A \cdot G \qquad (54)$$

Where the PV generator efficiency η_{PV} depends on the operating conditions and G is the global incident irradiance on the PV generator plane, which is calculated using the procedures described in the previous chapter. Dividing the previous equations and solving for P_{PV} yields

$$P_{PV} = P_{PV}^* \frac{G}{G^*} \frac{\eta_{PV}}{\eta_{PV}^*} \qquad (55)$$

Depending on the ratio ($\eta_{\mathrm{PV}}/\eta_{\mathrm{PV}}^*$) different models are available for calculating P_{PV}. For example, for an ideal PV generator $\eta_{\mathrm{PV}} = \eta_{\mathrm{PV}}^*$ and the corresponding maximum power is simply proportional to the incident irradiance.

$$P_{PV} = P_{PV}^* \frac{G}{G^*} \qquad (56)$$

PVlite uses the following simple approximation that includes both optical losses and temperature losses

$$\frac{\eta_{PV}}{\eta_{PV}^*} = \frac{G_{ef}}{G} [1 - CVPT(T_C - T_C^*)] \qquad (57)$$

Where G_{ef} is the effective irradiance on the PV generator plane, which is calculated as described in section 2-5-6.

Finally, the maximum power of the PV generator under real operating conditions is obatined as

$$P_{PV} = P_{PV}^* \frac{G_{ef}}{G^*} [1 - CVPT(T_C - T_C^*)] \qquad (58)$$

The parameter CVPT is the coefficient of variation of power with temperature, which in this equation should be included as a positive number and whose units are $\mathrm{^oC^{-1}}$. The parameter T_C^* is the cell temperature under STC ($T_C^* = 25^oC$) and T_C is the operating cell temperature, which is calculated from the ambient temperature T_a and the effective irradiance G_{ef} as

$$T_C = T_a + R_{th} \, G_{ef} \qquad (59)$$

Where R_{th} is the thermal resistance, given in $^oC \cdot m^2/W$, which depends on the mounting and ventilation of PV modules. By default, cell temperature is calculated using the well-know equation based on the nominal operation cell temperature, $NOCT$.

$$R_{th} = \frac{NOCT - 20}{800} \qquad (60)$$

For example, for $NOCT = 48^\circ C$ the previous equation yields R$_{th}$=0.035 $^\circ$C·m²/W, but any other value can be selected. Typical values for the thermal resistance R$_{th}$ are displayed in Table 5.

Mounting	R$_{th}$ [$^\circ$C·m²/W]
Well cooled	0.020
Free standing	0.021
Flat on roof	0.026
Façade integrated	0.054
On sloped roof	0.056

Table 5.   Typical values of the thermal resistance for several mounting of PV module [21]

If required, P_{PV} can be multiplied by a correction factor to add other power losses, such as those caused by the mismatch of PV modules or by the inaccuracy of MPP tracking.

Besides, it is assumed that all the modules of the PV generator are mounted in the same rack with equal orientation and inclination and that there are not neither horizon nor mutual shading losses caused by adjacent PV generators [22]

Finally, the value of P_{PV} can be further reduced by power losses caused by the total DC wiring P_{WDC}, which can be estimated as

$$P_{WDC} = \left(\frac{W_{DC}}{100 \cdot P_{PV}^*} \right) P_{PV}^2 \tag{61}$$

Where W_{DC} are total DC wiring losses under STC, expressed as a percentage of P_{PV}^*. For example, if $W_{DC} = 1\%$, the previous equation yields $P_{WDC} = 0.01 \cdot P_{PV}^*$ when $P_{PV} = P_{PV}^*$.

3-3 Inverter model

The inverter is modelled as power converter characterized by its power conversion efficiency η_I, which is defined as the ratio of the output AC power delivered to the load P_{AC} to the DC input power P_{DC}:

$$\eta_I = \frac{P_{AC}}{P_{DC}} = \frac{P_{AC}}{P_{AC} + Power\ losses} \tag{62}$$

Among other factors, η_I mainly depends on the normalized AC output power, p_{ac}, which is defined as $p_{ac} = P_{AC}/P_{I,NOM}$, where $P_{I,NOM}$ is the nominal inverter power. The power efficiency also slightly depends on the DC input voltage V_{DC}, with causes typical variations from 0.005 to 0.02 %/V.

For modeling purposes, inverter losses have been approximated using the following polynomial equation:

$$Power\ losses = C_0 + C_1 P_{AC} + C_2 P_{AC}^2 \tag{63}$$

Where coefficients C_0, C_1 and C_2 are constant parameters that must be fitted from the power efficiency curve provided by the inverter manufacturer or from experimental measurements.

These coefficients represent different power losses mechanism in the inverter: C_0 represents the power consumption of internal circuits, for example control circuits, when the loads are disconnected ($P_{AC} = 0$ and $\eta_I = 0$). The coefficient C_1 represents the losses that depend linearly on the current (e.g., voltage drop across diodes), and C_2 represents the losses that depend on the square of the current (e.g., resistive losses). To account for the efficiency dependence on the voltage, each one of these parameters could be approximated in a similar way as polynomial on V_{DC} ($C_i = a_{i0} + a_{i1} V_{DC} + a_{i2} V_{DC}^2$, where $i = 0, 1, 2$). As mentioned above, this dependence is usually negligible and it is not considered in the power efficiency model.

Power losses can also be expressed as a function of the normalized output power p_{ac} as:

$$Power\ losses = k_0 + k_1 p_{ac} + k_2 p_{ac}^2 \tag{64}$$

Where coefficients k_0, k_1 and k_2 can be directly fitted from the power efficiency curve or calculated from the previous parameters ($k_0 = C_0/P_{I,NOM}$, $k_1 = C_1$ and $k_2 = C_2 P_{I,NOM}$). Using these coefficients, the inverter power efficiency can be expressed as [23]

$$\eta_I(p_{ac}) = \frac{p_{ac}}{p_{dc}} = \frac{p_{ac}}{p_{ac} + (k_0 + k_1 p_{ac} + k_2 p_{ac}^2)} \tag{65}$$

Where $p_{dc} = P_{DC}/P_{I,NOM}$ is the normalized input power. The previous equation allows to obtain the power inverter efficiency and p_{dc} starting from the p_{ac}, which is the case when the AC power is known. At other times during simulations the starting data is p_{dc}. In these cases, p_{ac} can be obtained by solving the following equation

$$p_{dc} = p_{ac} + (k_0 + k_1 p_{ac} + k_2 p_{ac}^2) \tag{66}$$

Which is quadratic equation of p_{ac} whose solution is given by

$$p_{ac} = \frac{-(1 + k_1) + \sqrt{(1 + k_1)^2 - 4k_2(k_0 - p_{dc})}}{2k_2} \tag{67}$$

Where the condition $p_{dc} \geq k_0$ is necessary to ensure that $p_{ac} \geq 0$. If $p_{dc} < k_0$, p_{ac} must be set to zero.

3-4 Load profiles

The AC power at the inverter output P_{AC} can be used to supply AC loads of the system owner, if any, and to feed the utility grid in the case of grid-connected PV systems. For simulation purposes, it is necessary to indicate the load demand, which requires to know not only the total energy consumption during a given period, typically one year, but also the instantaneous variation of the power consumed by the AC loads.

For this purpose, the monthly mean of daily energy consumption L_{dm} can be distributed during each day using a normalized load profile, which indicates the fraction of L_{dm} consumed by the load in each instant. In an hourly basis, the power consumed by the load $P_{LOAD}(h)$ is obtained as

$$P_{LOAD}(h) = F(h) \cdot L_{dm} \qquad (h = 1, 2, \ldots 24) \tag{68}$$

Where F(h) is an hourly load factor that defines the fraction of L_{dm} consumed in each hour. As the integral of $P_{LOAD}(h)$ over one day is equal to L_{dm}, the sum of all these factors is equal to the unity.

$$\sum_{h=1}^{24} F(h) = 1 \tag{69}$$

For a constant load profile the load factors are equal to F(h) = 1/24 ≅ 0.042. In general, the load power is not constant and depends on user habits. For example, Table 6 shows two mean normalized load profiles of grid-connected dwellings, which are displayed in Figure 15 considering for denormalization that L_{dm} = 20 kWh.

Hour	Profile 1	Profile 2	Hour	Profile 1	Profile 2	Hour	Profile 1	Profile 2
1	0.048	0.043	9	0.048	0.042	17	0.034	0.041
2	0.047	0.041	10	0.043	0.047	18	0.034	0.038
3	0.044	0.041	11	0.039	0.047	19	0.036	0.036
4	0.042	0.039	12	0.037	0.048	20	0.039	0.036
5	0.042	0.038	13	0.036	0.048	21	0.043	0.038
6	0.041	0.038	14	0.035	0.045	22	0.050	0.041
7	0.042	0.038	15	0.035	0.044	23	0.053	0.045
8	0.045	0.038	16	0.035	0.043	24	0.052	0.045

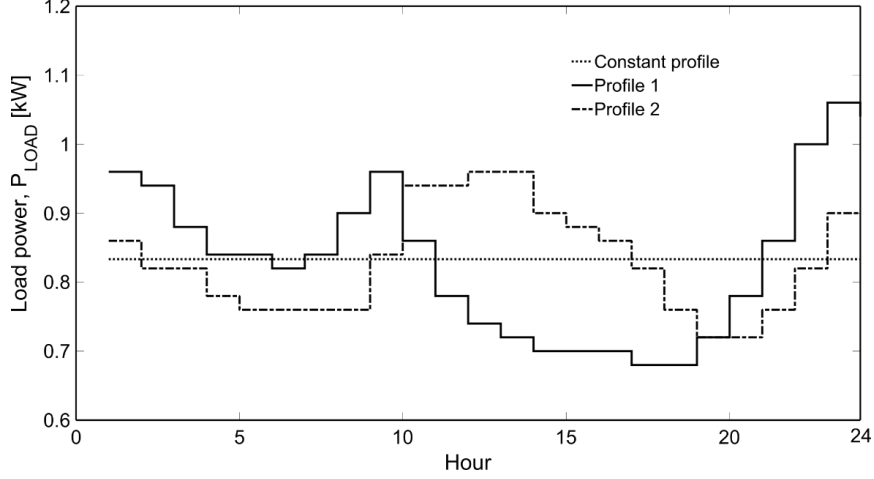Table 6.   Two typical mean normalized hourly load profiles of grid-connected dwellings.

Figure 15. Example of different load profiles with the same daily energy consumption (20 kWh).

3-5 System operation model

The grid-connected PV system displayed in Figure 14 is simulated as follows. First, the power at the inverter input P_{DC} is obtained as

$$P_{DC} = P_{PV} - P_{WDC} \tag{70}$$

Second, the power at the inverter output P_{AC} is obtained from P_{DC} using the inverter power efficiency model described in section 3-3.

$$P_{AC} = P_{I,NOM} \frac{-(1 + k_1) + \sqrt{(1 + k_1)^2 - 4k_2(k_0 - P_{DC}/P_{I,NOM})}}{2k_2} \tag{71}$$

Next, the AC power is recalculated by the program by subtracting the power losses caused by AC wiring P_{WAC}

$$P_{AC} = P_{AC} - P_{WAC} \tag{72}$$

Where P_{WAC} is calculated similarly to DC wiring losses as

$$P_{WAC} = \left(\frac{W_{AC}}{100 \cdot P_{I,NOM}} \right) P_{AC}^2 \tag{73}$$

Where W_{AC} are total AC wiring losses, which are expressed as a percentage of the nominal inverter power $P_{I,NOM}$.

Finally, the power exported to the grid P_{GRID} is calculated by substracting from P_{AC} the power consumed by AC loads

$$P_{GRID} = P_{AC} - P_{LOAD} \tag{74}$$

4 Stand-alone PV systems

4-1 Introduction

The present version of PVlite simulates stand-alone PV systems that supply AC loads through an inverter, with the configuration displayed in Figure 16. The system can be used for simulating a system with only DC loads setting the inverter efficiency to 100% ($\eta_I = 1$).

The models of the PV generator, the inverter and the load consumption profiles are the same described in the previous chapter.
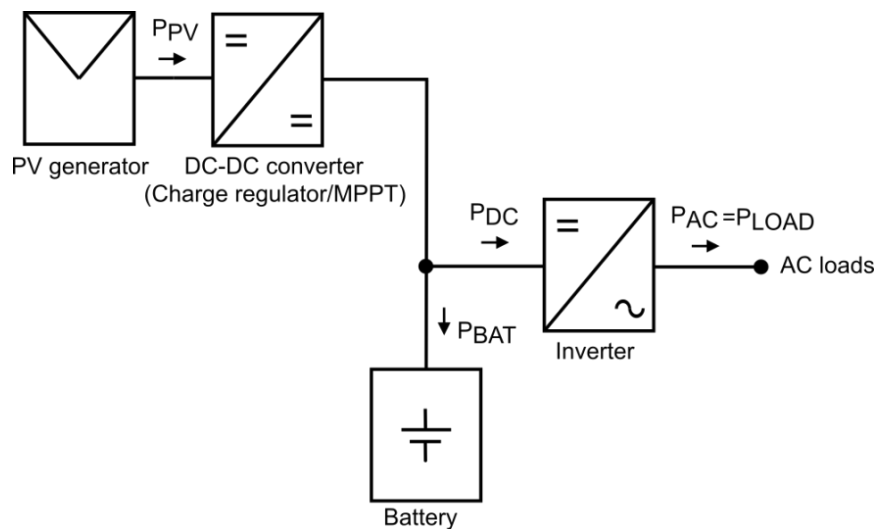

Figure 16. Stand-alone PV system configuration simulated in PVlite.

4-2 System operation model

The program calculates at each simulation step the PV power P_{PV} and the AC power demand P_{LOAD} according to the load consumption profile. Next, the battery power P_{BAT} is obtained as

$$P_{BAT} = P_{PV} - P_{DC} = P_{PV} - \frac{P_{LOAD}}{\eta_I} \tag{75}$$

Where P_{DC} is the power at the inverter input and η_I is the inverter power efficiency. P_{BAT} is positive when the battery is being charged, which occurs when the generation exceed the load demand ($P_{PV} > P_{DC}$). Or negative, when the PV power is not enough to supply the load demand ($P_{PV} < P_{DC}$) and the battery is being discharged.

Next, the instantaneous state of charge SOC, considering that the battery is fully charged at the beginning of the simulation, is calculated at any instant as

$$SOC(t) = 1 + \frac{\int \eta_{BAT} P_{BAT}(t)dt}{C_{BAT}} \qquad (76)$$

Where η_{BAT} is the battery charging efficiency, which is assumed that is equal to 100%, and C_{BAT} is the nominal capacity of the battery. The control strategy consists of disconnecting the PV generator when the state of charge reaches a given maximum ($SOCmax$), or disconnecting the inverter and AC loads when the state of charge decreases below a given minimum ($SOCmin$).

Besides power and efficiencies of the system components, the simulator calculates two figures of merit. First, the loss of load probability LLP, which is defined as the ratio of the energy deficit to the total energy demand. Second, the loss of load hours LLH, which indicates the fraction of time that the system shutdowns and fails to satisfy the load demand. The parameter LLH which coincides with the LLP if the load demand is constant.

The users guide provides additional details on the calculation of these parameters and related graphical tools, such as the construction of iso-reliability maps, with display contours of equal LLP as a function of the nominal PV power and the nominal capacity of the battery.

5 Water pumping PV systems

5-1 Introduction

The PV pumping water system simulated in PVlite is composed of a PV generator, a variable-frequency drive (VFD) and an AC centrifugal motorpump (see Figure 17).
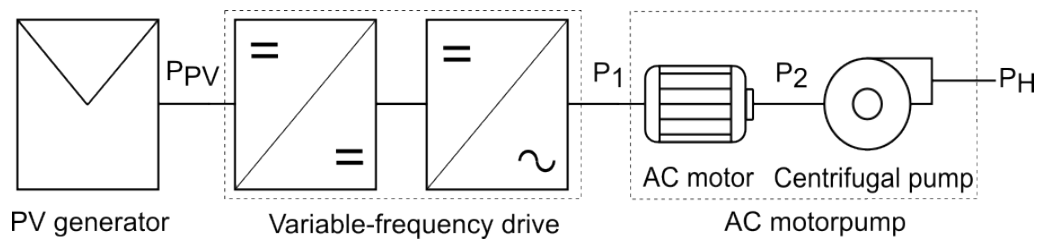

Figure 17. PV pumping system simulated in PVlite.

5-2 Characteristics and modeling of the water source

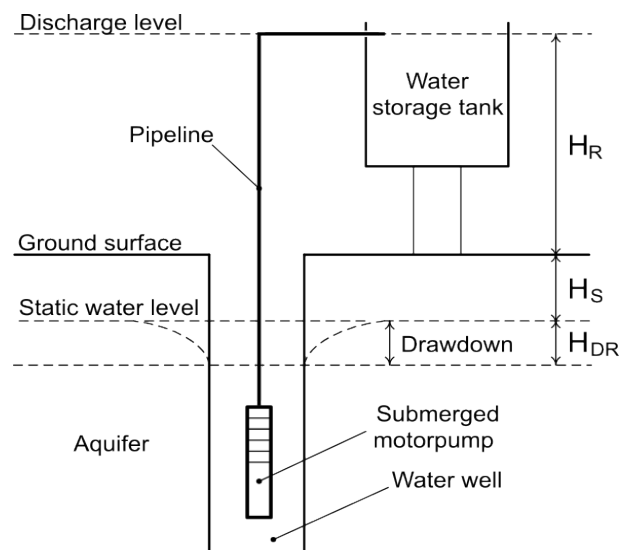Figure 18 shows the characteristics of the water source, where it is assumed that a submerged motor pump elevates the water from the well to a water storage tank.

Figure 18. Characteristics of the water source.

The static head H_S is defined as the distance from the ground surface to the surface of the water when no water is being pumped from the well. The static head can vary depending on the season but here it is assumed a constant value.

The distance from the ground surface to the point of injection on the water tank is indicated as H_R. In this version, the water tank capacity is considered infinite, which is equivalent to assume that the pumped water is consumed immediately.

When the water is being pumped from the well, the water level drops a certain distance called drawdown H_{DR}. The drawdown depends on the water flow Q, the well capacity, and the aquifer permeability, and can be approximated using the Jacob equation [25]

$$H_{DR} = k_{W1}Q + k_{W2}Q^2 \tag{77}$$

Where the parameters k_{W1} and k_{W2} are called, respectively, aquifer coefficient and well loss coefficient, which can be determined from on-site step-drawdown pumping tests. For that, it is usual to express the previous equation as

$$\frac{H_{DR}}{Q} = k_{W1} + k_{W2}Q \tag{78}$$

Which is the equation of straight line that allows fitting these coefficients from experimental data. The Figure 19 shows an example.
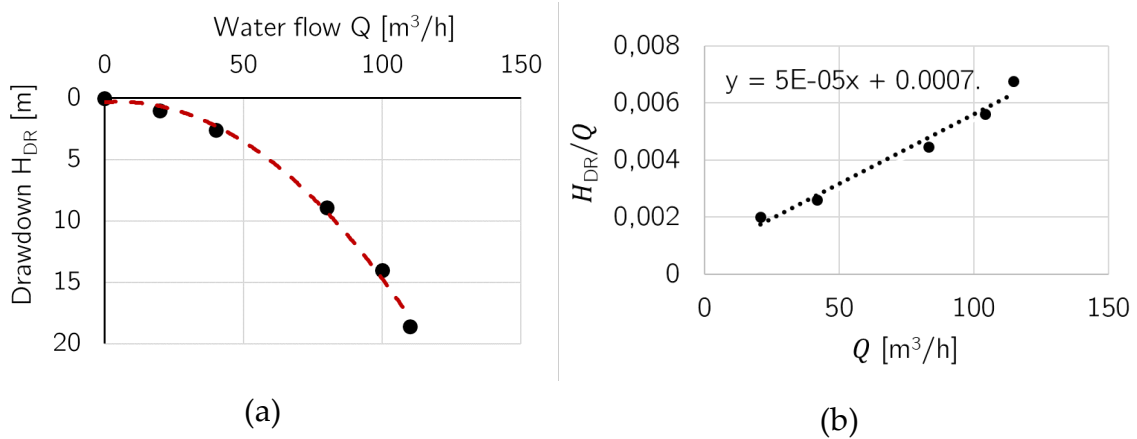

Figure 19. (a) Step-drawdown test, which consists of measuring the drawdown at different consecutive water flows. (b) Parameters fitting ($k_{W1} = 0.0007 \ m/(m^3/h)$ and $k_{W2} = 5 \cdot 10^{-5} \ m/(m^3/h)^2$).

When the drawdown test of the borehole is performed at one single constant flow Q_{test}, the drawdown is linearly approximated assuming that $k_{W2} = 0$ and calculating a value for k_{W1}, also called specific drawdown in $m/(m^3/h)$, as

$$k_{W1} = \frac{H_{DR}}{Q_{test}}$$

Besides of overcoming the total head, the pump must also provide power to compensate for the pressure losses caused by friction in pipelines and other elements. This friction losses can be expressed by an equivalent friction head H_F, which can be estimated using the Darcy-Weisbach equation.

$$H_F = \left(\frac{H_{F,rated}}{Q_{rated}^2} \right) \cdot Q^2$$

where Q is the water volumetric flow rate, or simply the flow, typically in units of cubic meters per hour, and $H_{F,rated}$ is the reference head loss, in meters, at the rated or nominal flow Q_{rated}.

The total manometric head, H_{MT} or simply H_T, as a function of the flow, also called the system curve (see Figure 20), is the sum of all geometric distances, drawdown and friction losses and it can be expressed as a third-order polynomial using the fitting coefficients k_{S0}, k_{S1} and k_{S2}.

$$H_T = H_S + H_R + k_{w1}Q + \left(k_{w2} + \frac{H_{F,rated}}{Q_{rated}^2} \right) Q^2$$

$$H_T = k_{S0} + k_{S1}Q + k_{S2}Q^2$$

Where:

$$k_{S0} = H_S + H_R$$
$$k_{S1} = k_{w1}$$
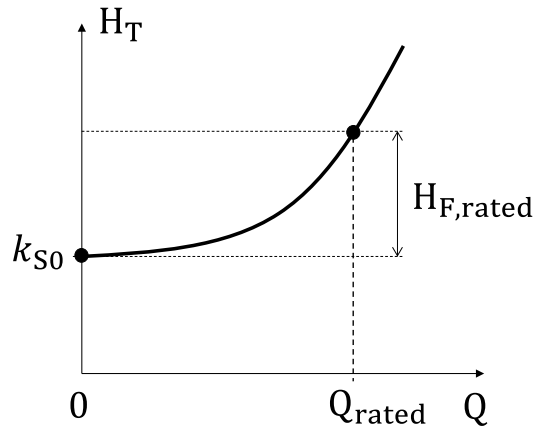$$k_{S2} = k_{w2} + \frac{H_{F,rated}}{Q_{rated}^2}$$

Figure 20. Example of system curve assuming a negligible drawdown.

5-3 System modeling

5-3-1 Performance curves of a centrifugal motorpump

The characteristics of centrifugal pumps are normally provided by a set of performance curves, which are defined at a nominal, or rated, rotational speed n_{NOM}.

Figure 21 displays an example of typical performance curves, which describes the variation of the following variables as a function of the flow rate Q, usually expressed m^3/h. In the top curve, H is the pump head, in metres, equivalent to the pump pressure (Pressure $= \rho \cdot g \cdot H$, in Pa, where where ρ is the water density in kg/m^3 and g is the acceleration of gravity 9.81 m/s^2).

The second graph displays the pump efficiency η_P and the motorpump efficiency η_{MP}. Typically, the pump manufacturer indicates the nominal operating point of the pump (Q_{rated}, H_{rated}) at the point where the pump efficiency reaches its maximum, which is called BEP (Best Efficiency Point).

Finally, in the bottom graph, P_1 is the electrical input power to the motor and P_2 is the mechanical power applied to the pump shaft. Both powers are also equal to the output power of the VFD and the motor, respectively (see Figure 17).
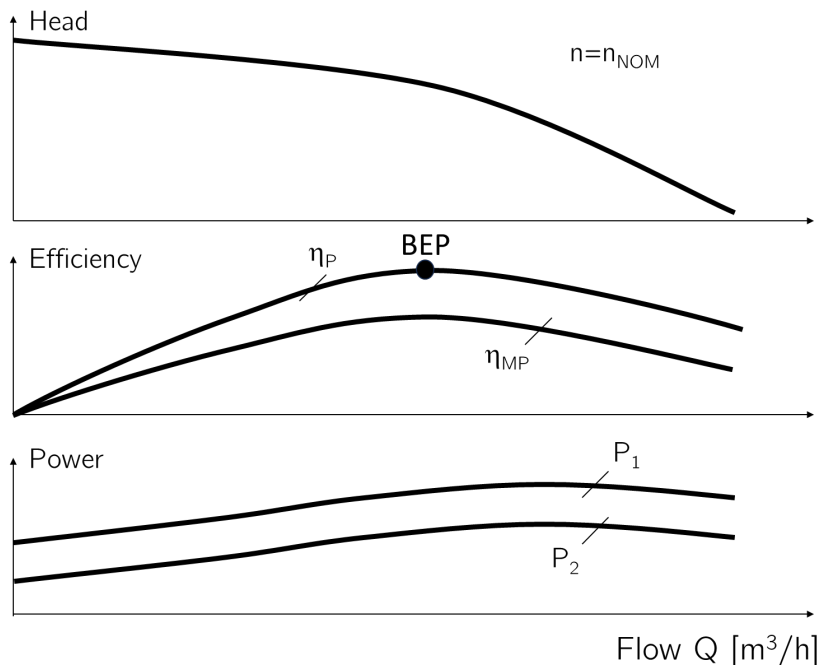

Figure 21. Typical set of performance curves of a centrifugal motorpump.

5-3-1-1 The head-flow curve H-Q

The curve displayed at the top of Figure 21 is called the head-flow curve of simply the pump curve. It can be observed that the flow increases as the head reduces and vice versa. For simulation purposes, the pump curve at the constant speed n_{NOM} can be approximated by a third-order polynomial

$$H = k_{H0} + k_{H1}Q + k_{H2}Q^2 \qquad (83)$$

Where k_{H0}, k_{H1} and k_{H2} are constant parameters that are fitted for each pump curve. Figure 22 shows an example of the parameter's fitting using the previous equation.
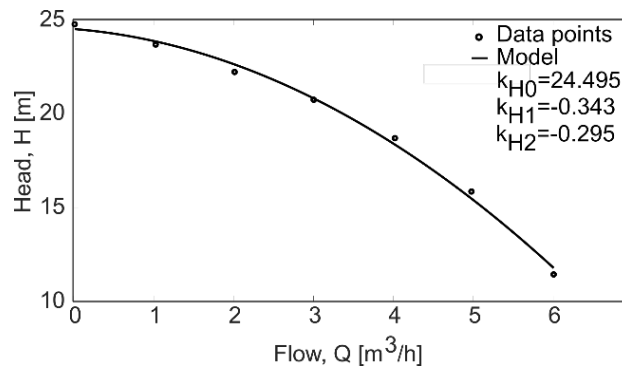

Figure 22. Fitting of pump curve at nominal speed.

5-3-1-2 Power curves

Similarly to the pump curve, P_1 and P_2 powers are approximated as a third-order polynomial as

$$P_1 = k_{P10} + k_{P12}Q + k_{P12}Q^2 \qquad (84)$$

$$P_2 = k_{P20} + k_{P22}Q + k_{P22}Q^2$$

Figure 23 shows an example of the parameter's fitting using the previous equations compared with experimental data points.
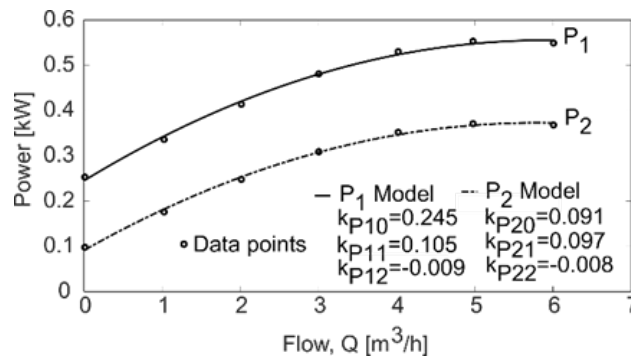

Figure 23. Fitting of the power curves of a commercial pump at nominal speed.

5-3-1-3 Efficiency curves

The efficiency of the pump η_P is defined by the ratio

$$\eta_P = \frac{P_H}{P_2} = \frac{2.725 \cdot Q \cdot H}{P_2} \tag{85}$$

Where P_H is the hydraulic power generated by the pump and P_2 is the mechanical power applied to the pump shaft.

The efficiency of the motor η_M is approximated as

$$\eta_M = \frac{P_2}{P_1} = \frac{P_2}{P_2 + (k_{m0} + k_{m1}P_2 + k_{m2}P_2^2)} \tag{86}$$

Where P_1 is the input power to the motor, which is equal to the AC output power of VFD, and k_{m0}, k_{m1} and k_{m2} are parameters that can be fitted using data provided by the manufacturer, which also specifies the nominal capacity of the motor $P_{2,NOM}$. Figure 24 shows an example of fitting of both pump and motor efficiency curves. The power efficiency of the motor pump η_{MP} is obtained as the product of both motor η_M and pump η_P efficiencies.

$$\eta_{MP} = \frac{P_H}{P_1} = \frac{P_2}{P_1} \cdot \frac{P_H}{P_2} = \eta_M \cdot \eta_P \tag{87}$$
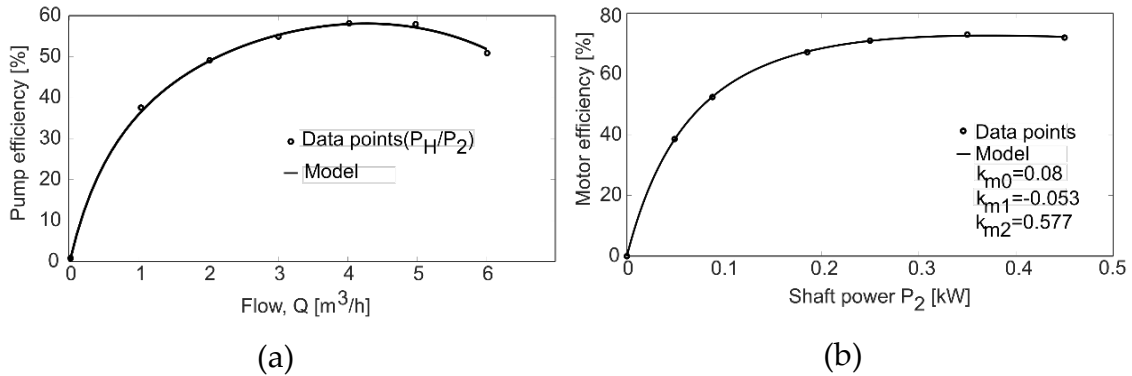

(a) (b)

Figure 24. Fitting of the efficiency curves of the pump at nominal speed (a) and the efficiency of the motor as function of its output power.

5-3-2 Efficiency of the VFD

To characterize the full conversion path of the PV system (see Figure 17), the efficiency of the VFD can be calculated as the ratio between P_1 and P_{PV}. Since the VFD is essentially an inverter, its efficiency can be modelled as described in section 3-3 as

$$\eta_{VFD} = \frac{P_1}{P_{PV}} = \frac{p_1}{p_1 + (k_0 + k_1 p_1 + k_2 p_1^2)} \tag{88}$$

Where $p_1 = P_1/P_{I,NOM}$, amd $P_{I,NOM}$ is the nominal power of the VFD.

5-3-3 The operating point of the pump

The operating point of the pump is obtained at the intersection of the system curve and the pump curve, as depicted in Figure 25. Under normal operation, this point is not constant because the speed of the pump continuously changes depending on the variation of the electrical input power P_1, which itself depends on the available PV power (the lower the irradiance, the lower the available power, the pump speed and the water flow).
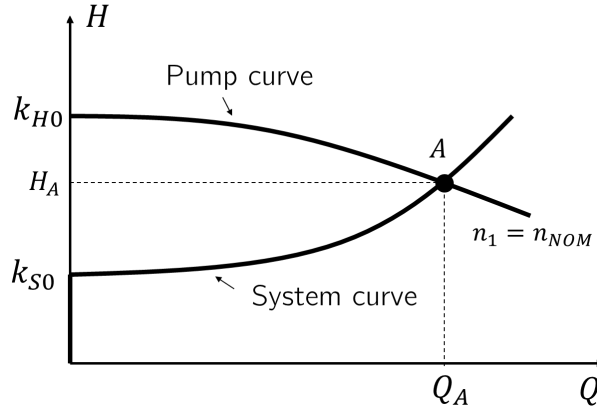

Figure 25. The operating point of the pump (Q_A, H_A) is obtained at the intersection of the pump curve and the system curve.

The pump operation under variable speed conditions can be described by means of the affinity laws, which are defined by the following three equations

$$\frac{Q_1}{Q_2} = \frac{n_1}{n_2} \qquad \frac{H_1}{H_2} = \left(\frac{n_1}{n_2}\right)^2 \qquad \frac{P_{2,1}}{P_{2,2}} = \left(\frac{n_1}{n_2}\right)^3 \qquad (89)$$

Where the subscripts 1 and 2 indicate, respectively, the value of flow Q, head H and shaft power P_2 at two different rotational speeds n_1 and n_2. From the first two equations it can be observed that the points (Q_1, H_1) and (Q_2, H_2) are contained on the same parabolic curve, which is usually called the affinity parabola.

$$\frac{H_1}{H_2} = \left(\frac{n_1}{n_2}\right)^2 = \left(\frac{Q_1}{Q_2}\right)^2 \qquad (90)$$

Besides, it can be shown that the pump efficiency is the same for all the points of this curve

$$\eta_{P,1} = \frac{P_{H,1}}{P_{2,1}} = \eta_{P,2} = \frac{P_{H,2}}{P_{2,2}} \qquad (91)$$

Hence, each affinity parabola defines a curve of iso-efficiency operating points. For example, the affinity parabola that crosses the point A in Figure 25 $(Q_1 = Q_A; H_1 = H_A)$, displayed in Figure 26, is expressed as:

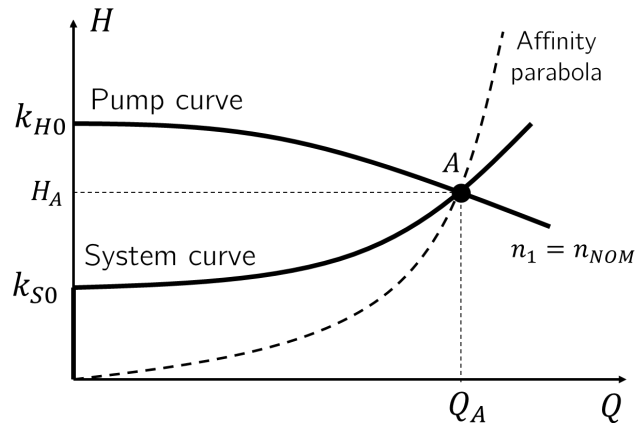$$H = \left(\frac{H_A}{Q_A^2}\right) Q^2 \tag{92}$$

Figure 26. The dashed curve is the affinity parabola that crosses the point A (Q_A, H_A). Ideally, all the points of this parabola have the same pump efficiency.

Using the affinity laws, the pump curve at a particular n_2 speed can be obtained as a function of $n_1 = n_{NOM}$ and the fitted parameters k_{H0}, k_{H1} and k_{H2} obtained for nominal speed.

$$H(n_2) = k_{H0}\left(\frac{n_2}{n_1}\right)^2 + k_{H1}\left(\frac{n_2}{n_1}\right)Q + k_{H2}Q^2 \tag{93}$$

Figure 27 shows an example of pump curves at different pump speeds. This figure also displays typical iso-efficiency curves of the motorpump ($\eta_{MP} = \eta_M \cdot \eta_P$), which have an elliptical form and tends towards zero when the flow and head decrease.
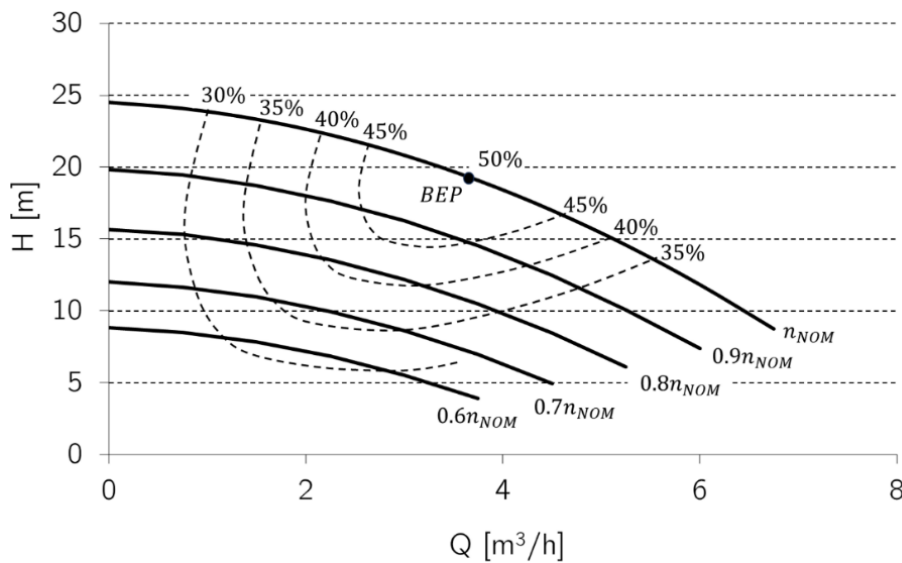

Figure 27. Variation of pump curve at different speeds and iso-efficiency motorpump curves (dashed lines).

Figure 28 displays how varies the operating point on the system curve at a reduced speed $n_2 < n_1 = n_{\text{NOM}}$, which moves from point A to point B reducing the water flow. It is worth pointing out that the transformation of the point B (Q_B, H_B) on the affinity parabola is not the point A but the point C (Q_C, H_C). Hence, the pump efficiency at point B is equal, according to affinity laws, to the pump efficiency at point C, which is directly obtained from the pump curve at the nominal speed $n_1 = n_{\text{NOM}}$.
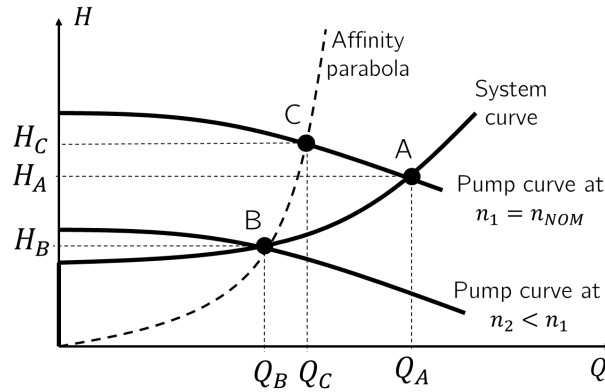

Figure 28. Variation of the operating point at a reduced speed. Ideally, the pump efficiency at point B is equal to the pump efficiency at point C, which are on the same affinity parabola.

The previous equation allows to determine the minimum speed for water pumping, which is obtained when the ordinate at the origin of the pump curve is equal to the total static head

$$k_{H0} \left(\frac{n_{MIN}}{n_{NOM}} \right)^2 = k_{S0} \ \rightarrow n_{MIN} = n_{NOM} \sqrt{\frac{k_{S0}}{k_{H0}}} \tag{94}$$

During the simulations, if $n \leq n_{MIN}$ the system stops. Besides, the system operation includes two additional speed limits. On one hand, the parameter called $RPMcool$ is the minimum speed required for motor cooling. If the speed decreases below this limit, the system is also stopped. On the other hand, the parameter called $RPMmax$ is the maximum speed of the pump. If the pump speed reaches this value, the output power of VFD will be limited to the given maximum $P_{1,max}$ that ensures the pump operates at its maximum speed.

5-3-4 Calculation of the Q-P₂ curve

For simulation purposes, it is convenient to obtain a relationship for calculating the output water flow Q, and related variables such as head, rotational speed, hydraulic power, etc., as a function of the shaft power P_2, which is directly obtained from the instantaneous PV power substracting the power

losses in the VFD and the motor. PVlite calculates this curve $Q - P_2$ for the specified system curve following the iterative procedure described below [4] .

1. Assume an initial flow equal to $Q = Q_B$ on the system curve (see Figure 28).
2. Calculate the corresponding head on system curve, $H_B = H_T(Q_B)$, to obtain the point B (Q_B, H_B).
3. Determine the affinity parabola that includes the point B.
4. Calculate the intersection of the affinity parabola and the pump curve at nominal speed to obtain the point C (Q_C, H_C) and the pump efficiency in this point using the pump efficiency at nominal speed.
5. The pump efficiency at the point B is equal to the pump efficiency at point C.
6. Calculate the hydraulic power at point B and, dividing by its pump efficiency, determine the corresponding shaft power at point B.

Repeating the previous sequence for different values of Q_B a set of discrete points for P_2 are obtained, which may be fitted with enough approximation using a two-order degree polynomial

$$P_2 = k_{Q0} + k_{Q1}Q + k_{Q2}Q^2 \tag{95}$$

Where k_{Q0}, k_{Q1} and k_{Q2} are fitting coefficients. Solving the previous equation for Q yields

$$Q = \begin{cases} \dfrac{-k_{Q1} + \sqrt{k_{Q1}^2 - 4k_{Q2}(k_{Q0}-P_2)}}{2k_{Q2}} & , \ P_2 \geq k_{Q0} \\ 0 & , \ P_2 \leq k_{Q0} \end{cases} \tag{96}$$

Where $P_2 = k_{Q0}$ is the minimum required shaft power to start the water pumping. Figure 29 shows and example of fitted $Q - P_2$ curves using the previous equations for several constant total heads.
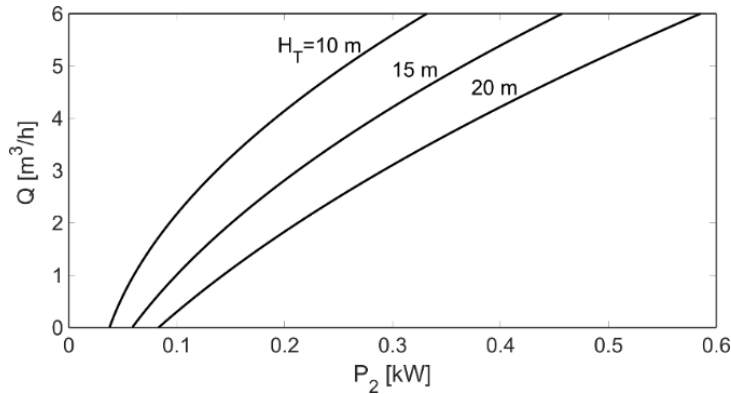

Figure 29. Typical shape of $Q - P_2$ curves obtained by simulation at several constant total heads.

PVlite calculates the water flow Q using two different algorithms, which can be selected by advanced users modifying the source code (script mainPump). The first one obtains Q from P_2 using the previous equation with fitted parameters k_{Q0}, k_{Q1} and k_{Q2}.

The second algorithm, which is executed by default in this version, uses a recursive algorithm that calculates Q from P_2 by iteration. Details of how this algorithm is implemented can be seen in the source code.

Finally, it is worth mentioning that manufacturers usually provide similar curves to those shown in Figure 29, but displaying the flow Q as a function of the input electrical power P_1. In other words, including the efficiency of the motor in the curves.

6 Hybrid PV systems

6-1 Introduction

The last PV application simulated in PVlite are hybrid systems that include one generator set (genset), composed of a fuel engine and an alternator, and one wind turbine. PVlite simulates a simple configuration, where both generators are connected to the DC bus of the stand-alone PV system described in chapter 4. Before of describing this system configuration, next section presents the implemented models for the generator set and the wind turbine.

6-2 Modeling of components

6-2-1 Generator set

The generator set is just modelled by a given nominal power $P_{GEN,nom}$, in kW, and its fuel consumption, which, for constant speed engine generators, is assumed to be linear using the following expression [26]

$$F = b_1 + b_2\, P_{GEN} \tag{97}$$

Where F is the fuel consumption in $\frac{L}{h}$, b_1 is the no-load fuel consumption or intercept parameter in $\frac{L}{h}$, b_2 is the marginal fuel consumption or slope parameter in $\frac{L}{kWh}$, and P_{GEN} is the output power of genset in kW. PVlite use the following equations for calculating b_1 and b_2 which include the dependence of these parameters on the nominal power of the generator $P_{GEN,nom}$.

$$b_1 = b_{0i} + b_{1i} \cdot P_{GEN,nom} \tag{98}$$

$$b_2 = b_{0s} + b_{1s} \cdot P_{GEN,nom}$$

Where the value of the coefficients are, by default, the following [26].

$$b_{0i} = 3.63719 \tag{99}$$
$$b_{1i} = 0.02031$$
$$b_{0s} = 0.25098$$
$$b_{1s} = -1.1827 \cdot 10^{-5}$$

The fuel consumption allows to calculate a related parameter call the heat rate HR, in $\frac{kWh}{L}$, which is an indication of the generator efficiency.

$$HR = \frac{P_{GEN}}{F} = \frac{P_{GEN}}{b_1 + b_2\,P_{GEN}}$$
(100)

Figure 30 shows and example of the fuel consumption and heat rate curves of an engine generator with $P_{GEN,nom} = 10kW$.
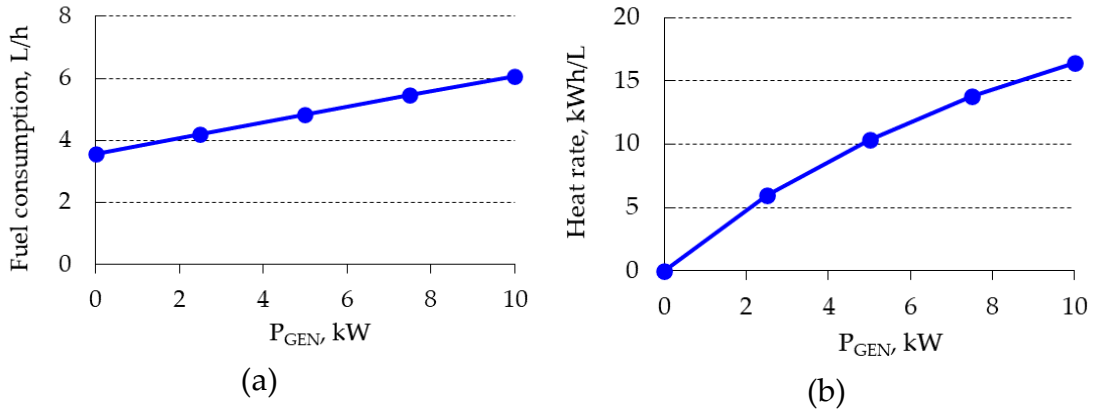

(a)   (b)

Figure 30. Fuel consumption (a) and heat rate (b) for an engine generator with $P_{GEN,nom} = 10kW$.

6-2-2 Wind turbine

The output power of the wind turbine P_{WIND} is modelled as cubic power curve of the wind speed v as [27]

$$P_{WIND} = \begin{cases} 0 & v \leq v_{ci}\ or\ v > v_{co} \\ C_{p,eq}(v^3 - v_{ci}^3) & v_{ci} < v < v_{nom} \\ P_{W,nom} & v_{nom} < v < v_{co} \end{cases}$$
(101)

Where

$P_{W,nom}$ Turbine rated power, kW.

$C_{p,eq} = \dfrac{P_{W,nom}}{v_{nom}^3 - v_{ci}^3}$ Equivalent power coefficient $C_{p,eq} = \frac{1}{2}\rho_w A_w C_p$, in $kW/(m/s)^3$. Being ρ_w the air density, typically $1.225\ kg/m^3$, A_w the turbine area and C_p the power coefficient, whose normal value is around 0.5.

v_{nom} Rated wind speed, m/s

v_{ci} Cut-in wind speed, m/s

v_{co} Cut-out wind speed, m/s

Figure 31 shows an example of the power curve model, where the calculated equivalent power coefficient is $C_{p,eq} \cong 0.023 \, kW/(m/s)^3$. Public data of several wind turbine models can be accessed through the NREL turbine archive [28]

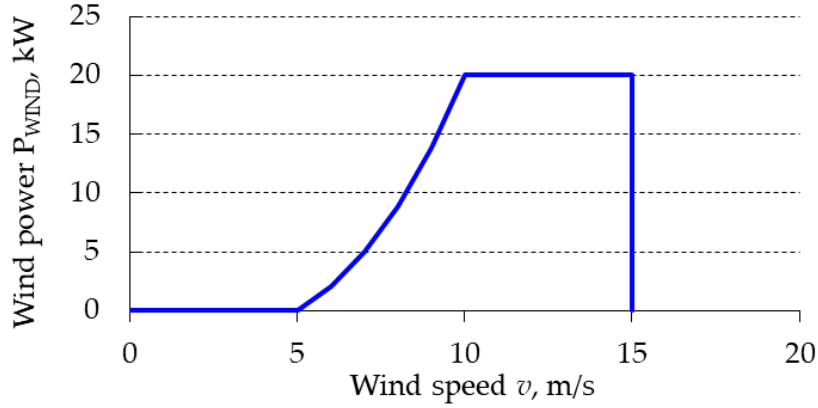*Figure 31. Example of power curve modeling of a wind turbine*
$(P_{W,nom} = 20 \, kW, v_{ci} = 5 \, \frac{m}{s}, \quad v_{nom} = 10 \, \frac{m}{s}, v_{co} = 15 \, \frac{m}{s})$

6-3 Hybrid configurations

As mentioned above, PVlite allows the of simulation hybrid systems with DC bus. It is assumed that both the genset and the wind turbine are always present in the hybrid system, although the wind power is only calculated when TMY files are selected for simulation, which contain the required wind speed input data. To remove either the genset or the wind turbine from simulation, its nominal power must be set to zero.

6-3-1 DC bus

The simulated DC bus configuration, also called series configuration, is displayed in Figure 32, where the PV generator, the genset and the wind turbine are connected in parallel in DC to provide a total power P_{TOT}.

$$P_{TOT} = P_{PV} + P_{GEN} + P_{WIND} \tag{102}$$

Essentially, the system operates as a stand-alone PV where the three input sources contributes to charging the battery. The input power P_{BAT} to the battery is given by

$$P_{BAT} = P_{TOT} - P_{DC} = P_{TOT} - \frac{P_{LOAD}}{\eta_I} \tag{103}$$

Where P_{DC} is the power at the inverter input, η_I is the inverter efficiency, and P_{LOAD} is the AC power consumption, which coincides with the output power of the inverter P_{AC} since AC wiring losses are negligible.

The AC/DC power converters that transform AC power from the genset and the wind turbine into DC power are considered ideal, i.e., their power efficiency is assumed to be 100%.

Depending on the design and control strategy of the hybrid system, the genset can be also directly connected to the AC loads, for example, to supply the peak load demand or operated an emergency backup in the case of an inverter breakdown.

For simulations, it is assumed that the inverter must be sized to supply the peak load AC demand and the genset is only connected for charging the battery, operating at its nominal power, when the state of charge SOC decreases below a certain minimum level specified by the user ($SOCstart$). And it remains in operation until the battery recovers until a given SOC level ($SOCstop > SOCstart$). Hence, the system provides a continuous energy service to the AC loads and $LLP = LLH = 0$.
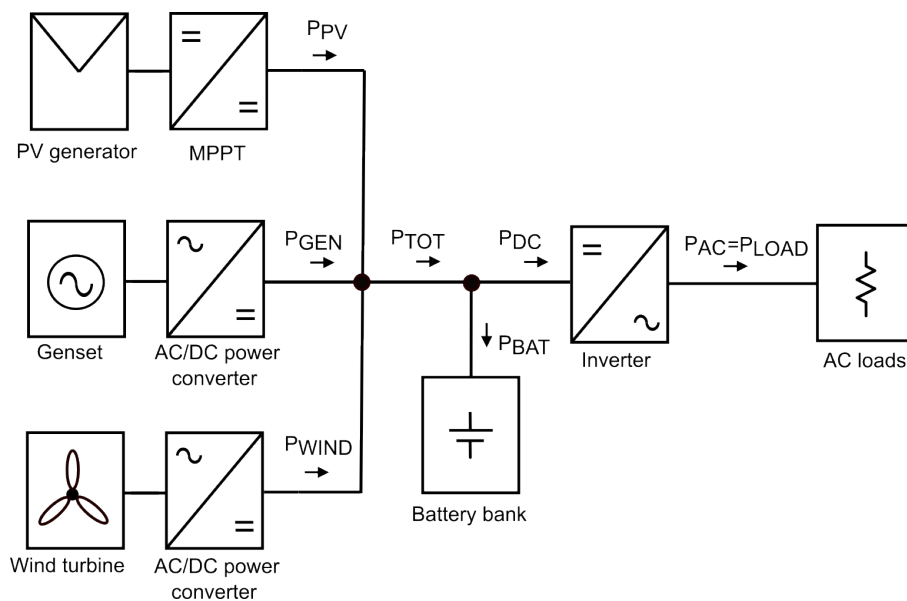

Figure 32. Hybrid system with DC bus.

References

[1] J. Muñoz, L. Marroyo, M. Collares-Pereira, N. Tyutyuyndzhiev, M. Conlon, A. Elmoussaoui, B. Wilkin. An Open-Source Simulation Tool of Grid-Connected PV Systems. 28th European Photovoltaic Solar Energy Conference and Exhibition, pages 3882–3887. https://www.doi.org/10.4229/28thEUPVSEC2013-5BV.4.18

[2] J. Muñoz and P. Díaz. A virtual photovoltaic power systems laboratory. IEEE EDUCON 2010 Conference, Madrid, Spain, 2010, pp. 1737-1740, https://www.doi.org/10.1109/EDUCON.2010.5492411.

[3] J. Muñoz. SISIFO, a PHP version of IESPRO. Translated from Matlab© to PHP by A. Makibar and J. M. Carrillo. https://github.com/javiermunozcano/SISIFO.

[4] Muñoz J., Carrillo J.M., Martinez-Moreno F., Carrasco L.M., Narvarte L. Modeling and Simulation of Large PV Pumping Systems. 31st European Photovoltaic Solar Energy Conference and Exhibition, 2925 – 2928 https://doi.org/10.4229/EUPVSEC20152015-6AV.5.42

[5] Photovoltaic Geographical Information System (PVGIS) https://re.jrc.ec.europa.eu/pvg_tools/en/

[6] National Solar Radiation Database (NSRDB) https://nsrdb.nrel.gov/

[7] J. W. Spencer. Fourier series representation of the position of the Sun. Search 2 (5), 172 (1971).

[8] M. Iqbal. An Introduction to Solar Radiation. Academic Press, 1983. https://doi.org/10.1016/B978-0-12-373750-2.50001-X

[9] E. Lorenzo. Energy Collected and Delivered by PV Modules, in: Luque, A., Hegedus, S. (Eds.), Handbook of Photovoltaic Science and Engineering. John Wiley & Sons, Ltd, pp. 984–1042., 2011. https://doi.org/10.1002/0470014008.ch20

[10] B. Liu and R. Jordan. The interrelationship and characteristic distribution of direct, diffuse and total solar radiation. Solar Energy 4 (3), 1-19 (1960). https://doi.org/10.1016/0038-092X(60)90062-1

[11] J.K Page. The estimation of monthly mean values of daily total shortwave radiation on vertical and inclined surfaces from sunshine records for latitudes 40°N-40°S. Proceedings U.N. Conference on New Sources of Energy 1961, 378-390.

[12] M. Collares-Pereira, and A. Rabl. The Average Distribution of Solar Radiation-correlations Between Diffuse and Hemispherical and Between Daily and Hourly Insolation Values. Solar Energy 22, no. 2 (1979): 155-164. https://doi.org/10.1016/0038-092X(79)90100-2

[13] D.G. Erbs, S.A. Klein, J.A. Duffie. Estimation of the Diffuse Radiation Fraction for Hourly, Daily and Monthly-average Global Radiation. Solar Energy 28, no. 4 (1982): 293-302. https://doi.org/10.1016/0038-092X(82)90302-4

[14] M.H. Macagnan, E. Lorenzo, C. Jimenez. Solar radiation in Madrid International Journal of Solar Energy 16, no. 1 (May 1994): 1-14. https://doi.org/10.1080/01425919408914262

[15] R.J. Aguiar, M. Collares-Pereira, J.P. Conde. Simple procedure for generating sequences of daily radiation values using a library of Markov transition matrices. Solar Energy, Volume 40, Issue 3, 1988, Pages 269-279, https://doi.org/10.1016/0038-092X(88)90049-7

[16] J.E. Hay, D.C. McKay. Estimating Solar Irradiance on Inclined Surfaces: A Review and Assessment of Methodologies. International Journal of Solar Energy 3, no. 4–5 (1985): 203–240. https://doi.org/10.1080/01425918508914395

[17] R. Perez, R. Seals, P. Ineichen, R. Stewart, D. Menicucci. A New Simplified Version of the Perez Diffuse Irradiance Model for Tilted Surfaces. Solar Energy 39, no. 3 (1987): 221–231. https://doi.org/10.1016/S0038-092X(87)80031-2

[18] C. Rigollier, O. Bauer, L. Wald. On the Clear Sky Model of the ESRA — European Solar Radiation Atlas — with Respect to the Heliosat Method. Solar Energy 68, no. 1 (2000): 33–48. https://doi.org/10.1016/S0038-092X(99)00055-9

[19] Martin, N., and J.M. Ruiz. Calculation of the PV Modules Angular Losses Under Field Conditions by Means of an Analytical Model. Solar Energy Materials and Solar Cells 70, no. 1 (December 2001): 25-38. https://doi.org/10.1016/S0927-0248(00)00408-6

[20] Martín, N., Ruiz, J.M., 2005. Annual angular reflection losses in PV modules. Progress in Photovoltaics: Research and Applications 13, 75–84. https://doi.org/10.1002/pip.585.

[21] Skoplaki E., Palyvos J.A., 2009. Operating temperature of photovoltaic modules: A survey of pertinent correlations. Renewable Energy, Volume 34, Issue 1, Pages 23-29. https://doi.org/10.1016/j.renene.2008.04.009

[22] Martínez-Moreno, F., J. Muñoz, and E. Lorenzo. Experimental Model to Estimate Shading Losses on PV Arrays. Solar Energy Materials and Solar Cells 94, no. 12 (December 2010): 2298-2303. https://doi.org/10.1016/j.solmat.2010.07.029

[23] M. Jantsch, H. Schmidt, J. Schmid. Results of the concerted action on power conditioning and control. 11th European Photovoltaic Solar Energy Conference 1992: 1589-1592.

[24] Muñoz, J., Martínez-Moreno, F. and Lorenzo, E. (2011), On-site characterisation and energy efficiency of grid-connected PV inverters. Prog. Photovolt: Res. Appl., 19: 192-201. https://doi.org/10.1002/pip.997

[25] Jacob, C.E., 1946. Drawdown test to determine effective radius of artesian well. Proc. Am. Soc. Civ. Eng. 72, 629–646. https://doi.org/10.1061/TACEAT.0006033

[26] Giles, P., Ross, M., Sumanik, S., 2020. Modelling Prime Diesel Electric Generator Fuel Consumption across Genset Sizings. 2020 IEEE Electric Power and Energy Conference (EPEC), pp. 1–8. https://doi.org/10.1109/EPEC48502.2020.9320082

[27] Carrillo, C., Obando Montaño, A.F., Cidrás, J., Díaz-Dorado, E., 2013. Review of power curve modelling for wind turbines. Renewable and Sustainable Energy Reviews 21, 572–581. https://doi.org/10.1016/j.rser.2013.01.012

[28] NREL Turbine Archive. https://nrel.github.io/turbine-models/